

AMERICAN UNIVERSITY OF BEIRUT

REAL-TIME ESTIMATION OF THE MASS
AND INERTIA TENSOR OF QUADROTORS
FOR CONTROLLER MAPPING

by

MOHAMAD ABDELKADER DHAYBI

A thesis

submitted in partial fulfillment of the requirements
for the degree of Master of Engineering
to the Department of Electrical and Computer Engineering
of the Faculty of Engineering and Architecture
at the American University of Beirut

Beirut, Lebanon
February 2014

AMERICAN UNIVERSITY OF BEIRUT

REAL-TIME ESTIMATION OF THE MASS AND INERTIA
TENSOR OF QUADROTORS FOR CONTROLLER MAPPING

by
MOHAMAD ABDELKADER DHAYBI

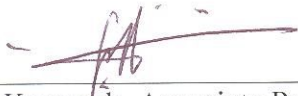
Approved by:



Dr. Naseem Daher, Assistant Professor

Advisor

Electrical and Computer Engineering



Dr. Fadi Karameh, Associate Professor

Member of Committee

Electrical and Computer Engineering



Dr. Daniel Asmar, Associate Professor

Member of Committee

Electrical and Computer Engineering

Date of thesis defense: November 21, 2019

AMERICAN UNIVERSITY OF BEIRUT

THESIS, DISSERTATION, PROJECT RELEASE FORM

Student Name: Dhaybi Mohamad Abdelkader
Last First Middle

Master's Thesis Master's Project Doctoral Dissertation

I authorize the American University of Beirut to: (a) reproduce hard or electronic copies of my thesis, dissertation, or project; (b) include such copies in the archives and digital repositories of the University; and (c) make freely available such copies to third parties for research or educational purposes.

I authorize the American University of Beirut, to: (a) reproduce hard or electronic copies of it; (b) include such copies in the archives and digital repositories of the University; and (c) make freely available such copies to third parties for research or educational purposes after: **One** ___ year from the date of submission of my thesis, dissertation or project.
Two ___ years from the date of submission of my thesis , dissertation or project.
Three ___ years from the date of submission of my thesis , dissertation or project.

Mohamad Dhaybi December 6, 2019
Signature Date

This form is signed when submitting the thesis, dissertation, or project to the University Libraries

Acknowledgements

Special thanks and respect for Professor Naseem Daher for his advise and guidance throughout the master's program. It's a great pleasure that he accepts my sincere gratitude for his help and supervision. I would also like to thank the members of my thesis committee, Prof. Fadi Karamah and Prof. Daniel Asmar, who provided me with enough support to make this project possible.

I would like to express my recognition and gratitude to my family, who were always there to support and comfort me no matter how difficult things got.

An Abstract of the Thesis of

Mohamad Abdelkader Dhaybi for Master of Engineering
Major: Electrical and Computer Engineering

Title: Real-time Estimation of the Mass and Inertia Tensor of Quadrotors for
Controller Mapping

The expanding need for UAVs to carry payloads with grasping abilities requires developing and improving the motion control systems of these aerial robots. Providing UAVs, such as quadrotors, with grasping abilities requires their ability to transport payloads in optimal time, minimal energy consumption, in addition to risk lessening in cases of dangerous missions, and many other advantages. This thesis aims at devising an online estimation scheme of the varying quadrotor's parameters as it picks up and manipulates a payload. In particular, the mass and the moment of inertia tensor of the quadrotor are estimated in real-time, while subjected to an additional payload, by analyzing the acquired input-output data in a direct closed-loop fashion and using its rigid body dynamic model. A modified version of the recursive least squares (RLS) method is leveraged for the proposed real-time estimation in this work. While most existing methods assume symmetry of the inertia tensor matrix and disregard its off-diagonal elements, which affects the control system's performance due to the disparity between the predicted model and the physical plant, in this work all of the inertia tensor parameters along with the quadrotor's changing mass are estimated and passed to the control system to achieve enhanced tracking performance. Covariance resetting is integrated into the estimation algorithm to increase its convergence rate and accuracy. Physical constraints are also used to attain consistent and rational estimates of the inertia tensor matrix. The proposed identification scheme is validated in numerical simulations and experimentation on the Quanser 3 DOF Hover and on a real-life quadrotor, the Quanser QBall-2. The obtained results demonstrate the accuracy and convergence rate of the designed estimator, paving the way in front of its integration into an adaptive control system. This system identification scheme is a main building block for future work that involves a controller mapping scheme, which calculates new control actions for the updated

system using the differential flatness property of quadrotors.

Contents

Acknowledgements	v
Abstract	vi
1 Introduction	1
2 Literature Review	3
3 System Modeling	7
3.1 Coordinate Frame:	7
3.2 Rigid Body Dynamics:	8
4 System Identification	11
4.1 Persistence of Excitation	13
4.2 Recursive Least Squares	13
4.3 Covariance Resetting	14
4.4 Physical feasibility of inertial parameters identification	16
5 Experimental Implementation	18
5.1 3 DOF Hover	18
5.1.1 Simulation Results on the 3 DOF Hover	25
5.1.2 Experimental Validation	29
5.2 QBall-2 Quadrotor	30
5.2.1 Simulation Results	32
5.2.2 Experimental Validation	42
6 Conclusion	52

List of Figures

3.1	Quadrotor free body diagram	8
4.1	open-loop and closed-loop identification	11
5.1	Quanser 3 DOF Hover	19
5.2	3 DOF Hover's direct closed-loop identification scheme	20
5.3	Infrared obstacle sensor module (RKI-3141)	21
5.4	Infrared obstacle sensor mounted on the hover platform	21
5.5	Vernier double range force sensor used for c_f identification	23
5.6	Identification of thrust coefficient c_f	23
5.7	Estimates of the inertia tensor diagonal elements, in simulation, with and without covariance resetting.	26
5.8	Power spectral densities (PSD) of the input torques in simulation	26
5.9	Added mass to the hover platform	28
5.10	Estimates of the inertia tensor diagonal elements, in experiment, with and without covariance resetting	28
5.11	Power spectral densities (PSD) of the input torques in experiment	29
5.12	Qball2 quadrotor's command system [1]	30
5.13	Battery drain effect model	32
5.14	QBall-2 inertia tensor identification scheme.	33
5.15	Quadrotor's mass estimation in numerical simulation	34
5.16	Non filtered torque Vs. roll measured acceleration in simulation	34
5.17	Filtered torque Vs. roll measured acceleration in simulation	34
5.18	Non filtered torque Vs. pitch measured acceleration in simulation	35
5.19	Filtered torque Vs. pitch measured acceleration in simulation	36
5.20	Detected error for covariance resetting in simulation	36
5.21	I_{xx} estimation auto-covariance in simulation	37
5.22	I_{yy} estimation auto-covariance in simulation	37
5.23	I_{zz} estimation auto-covariance in simulation	38
5.24	Estimates of the inertia tensor diagonal elements in simulation	38
5.25	Power spectral densities (PSD) of the input torques in simulation	39
5.26	Eigenvalues of J	40
5.27	Eigenvalues of Y before correction	40
5.28	Eigenvalues of Y after correction	41

5.29	Quadrotor's mass estimation in numerical simulation	42
5.30	Detected error for covariance resetting in experiment	42
5.31	Output roll ϕ angle	43
5.32	Output pitch θ angle	44
5.35	Filtered torque Vs. roll measured acceleration in experimentation	44
5.33	Output yaw ψ angle	45
5.36	Filtered torque Vs. roll measured acceleration (Zoomed) in exper- imentation	45
5.34	Non filtered torque Vs. roll measured acceleration in experimentation	46
5.37	Non filtered torque Vs. pitch measured acceleration in experimen- tation	46
5.38	Filtered torque Vs. pitch measured acceleration	47
5.39	Filtered torque Vs. pitch measured acceleration (Zoomed) in ex- perimentation	47
5.40	Filtered torque Vs. yaw measured acceleration in experimentation	48
5.41	Filtered torque Vs. yaw measured acceleration (Zoomed) in ex- perimentation	48
5.42	I_{xx} estimation auto-covariance in experimentation	49
5.43	I_{yy} estimation auto-covariance in experimentation	49
5.44	I_{zz} estimation auto-covariance in experimentation	50
5.45	Estimates of the inertia tensor diagonal elements in experiment .	50
5.46	Power spectral densities (PSD) of the input torques in experiment	51

Chapter 1

Introduction

Due to their numerous and various applications in civil and military areas, vertical take-off and landing (VTOL) unmanned aerial vehicles (UAVs), and especially quadrotors, have gained a wide interest from academic, industrial, and governmental institutes [2]. In fact, quadrotors provide many advantages such as small size, mechanical simplicity, high maneuverability, and ability to carry a large array of sensing elements. These benefits make quadrotors suitable for disasters rescue missions and supervision tasks such as security and road traffic supervision [3]. Further advanced applications could be repair and maintenance of high-voltage overhead power lines and wind turbines, service of agricultural crops in remote agricultural lands, and geological sampling of volcanic rock [4]. A quadrotor is an under-actuated system with four rotors, each producing a thrust force in the normal direction of the air-frame. Four basic motions are attained including normal thrust (translation) and three rotations: roll, pitch, and yaw. The system is open-loop unstable, which emphasizes the value of developing an accurate model for the flight control system design and for simulation using physical laws or by system identification approaches.

Furthermore, given the various quadrotor applications, its mass and moment of inertia change while carrying payloads during its missions, which stresses the importance for an efficient online system identification scheme to keep track of these changes. This is crucial for the design of an adaptive control system that can cope with the system's variations. From a control system design standpoint, multiple strategies have been developed previously. For instance, feedback linearization was used in [5], nonlinear control design was used in [6] for precise trajectory tracking, and robust control was used in [7] for trajectory following in the existence of disturbances. However, all of the previously mentioned controllers assumed perfect symmetry of quadrotors, which is not always valid.

Due to strong couplings and high nonlinearity, several methods have been proposed to identify quadrotor systems; these techniques can be divided between approximating the transfer functions of the quadrotor dynamics and estimating the model parameters. In addition, parameter estimation schemes are divided

between offline and online estimation.

In principle, system identification can be achieved in both open-loop and closed-loop configurations. In open-loop, input is directly given to the quadrotor without the presence of a feedback loop, and then by measuring the output and using the prediction error minimization (PEM) method, the system is identified [8]. However, the instability of the open-loop model of quadrotors causes high sensitivity of the error function, thus deeming the open-loop identification process impossible. Furthermore, operating the unstable quadrotor in open-loop could damage the platform and the surrounding in which the experiments are executed. Thus, for safety and efficiency of operation requirements, quadrotors need to be identified in closed-loop.

The rest of this thesis document is structured as follows. In section 2, previous works on quadrotor system identification are presented. The dynamic model of quadrotor systems is described in section 3. Section 4 explains the proposed system identification methodology. Section 5 includes validation of the estimation approach through numerical simulations and experiments on an actual quadrotor platform. Finally, conclusions and future work are provided in Section 6.

Chapter 2

Literature Review

Dynamic modeling is the first and key step for control system design and accurate numerical simulations. In general, system models are derived from first principles, physical insights, and system identification using input-output data. For a quadrotor vehicle, traditional flight mechanics can be utilized to obtain its dynamic model, which features coupling between the states and nonlinearities that complicate the control system design process. As an alternative solution, system identification schemes are effective in proposing a model structure and identifying its associated parameters. However, the quadrotor system's nonlinear model along with the closed-loop identification are open problems that should be tackled while identifying such system.

Considering an off-white model approach, which blends black-box identification with white-box modelling based on physical principles, a set of parameters in the quadrotor's nonlinear model are taken directly from measurements and custom experimental platforms, and blended with three-dimensional (3D) models of all of its parts generated via computer aided design (CAD). In [9], the identification problem of a quadrotor UAV was treated in three steps. In the first step, the complete quadrotor's dynamic model was obtained via the Newton formalism and expressed in a form suited for identification of the pertinent dynamic parameters. In the second step, the inertia matrix, the aerodynamic friction coefficients, and the translation drag coefficients were identified via the Levenberg-Marquardt optimization method using four-wires and two-wires rotational pendulums. The rotor parameters were estimated using the quadratic optimization method based on motor input and rotor angular speed measurements. In the third step, the estimated parameters were validated by comparing the performance of the same PID controller applied to the estimated model and the real system. In [10] and [11], experimental identification was used to compute the quadrotor's model parameters such as the thrust coefficient, drag coefficient, and the inertia matrix. In [12], the mass (in Kilograms) was calculated for each part and the full weight of the assembly was computed using the volume and density of every part utilizing CAD modeling (SolidWorks) based on mass calculation and library of materi-

als. Furthermore, the symmetric mass distribution was not assumed and the full inertia matrix was computed using SolidWorks' *Mass Properties* utility.

Other approaches for quadrotor identification are based on steel-grey models, where its nonlinear dynamic equations are linearized around a working point such as the hovering regime. For instance, the authors in [13] identified a linear discrete state-space model of the quadrotor using PEM. However, although such model is useful for controller design, its linearity tends to decrease the fidelity of the simulation and narrow its validity to a small range around the linearization point. In [14], several model structures for the quadrotor system were suggested such as ARX (Autoregressive with External Input), ARMAX (Autoregressive Moving Average eXogenous), OE (output error), and BJ (Box-Jenkins). The ARMAX model was chosen due to its numerical stability and unbiasedness. By adopting an order of two and using the prediction error minimization (PEM) method, the parameters of the model were estimated. In [15], the quadrotor system was divided to sub models: a SISO model for the altitude and MIMO models for the three angular velocities of the quadrotor. Each sub model was given an ARX structure and recursive least squares (RLS) was used to estimate the models parameters from hovering data. However, these estimations can only be used to design controllers that are effective near the hovering operation condition.

On the other hand, a frequency-domain system identification method was used in [16] to obtain a linear representation of the quadrotor dynamics. The acquired frequency response data was validated by evaluating its coherence, which is an indication of how well the output and input data are correlated. To apply the identification method, the transfer functions of each axis was first acquired, followed by state-space representations, and complete system analysis. The excitation signal was chosen to be periodic in order to minimize leakage in the computation of the frequency spectra. Frequency domain identification was also used in [17] to estimate angular motions transfer functions of a quadcopter hover platform.

In [18], a quadrotor's moments of inertia and the rotor inertia parameters were estimated using an unscented Kalman filter (UKF) while the aerodynamic parameters were assumed to be experimentally identified in advance. However, the structure of the quadrotor was assumed to be symmetrical with respect to its axes. This assumption ignores the off-diagonal elements of the inertia matrix, and the proposed method only estimated the diagonal elements, which is not always the case in a real system with a payload. Furthermore, the parameters were estimated offline after collecting experimental data and no validation of the identification was done other than the convergence of the unscented Kalman filter. In [19], the inertia matrix of the quadrotor, the rotor inertia, and the aerodynamic parameters were identified. The nonlinear model parameters were analytically approximated initially and then they were refined using PEM for closed-loop data. These parameters were then used to design a linear quadratic optimal tracker. Nonetheless, the off-diagonal elements of the inertia tensor were also considered

null. In [20], an Assorting Reconfiguring Equipping Solving (ARES) algorithm was used to identify the full inertia tensor parameters of a quadrotor using an algebraic solution. Although the asymmetric terms were not considered as null, the estimation was very sensitive to sensor noise since it did not use an optimization scheme for robustness against measurements uncertainties. Furthermore, the method was used to identify the system’s inertia tensor in an offline fashion, thus it was not validated for online estimation. Mass estimation of the quadrotor was performed and validated using experimental data in [21], where three offline estimation methods were compared and the instrumental variables method was found to yield the most accurate estimates for closed-loop identification.

Artificial intelligence (AI) was also used to find the system’s unknown parameters. For instance, Liu Yang and Jinkun Liu [18] used particle swarm optimization (PSO) swarm intelligence algorithm to estimate the inertia parameters of the quadrotor. Furthermore, an adaptive genetic algorithm (GA) was proposed in [22] to perform parameter identification of a small unmanned aerial rotorcraft’s linear model. In [23], a black-box model that uses a neural network to learn the dynamics of the quadrotor was attempted. Each translational velocity and Euler rate was given a net in the nonlinear autoregressive network with exogenous inputs (NARX) architecture. The result showed that the black-box neural network model can predict both the roll and pitch with very good accuracy, but with a poor one for the yaw rate, which should be improved by creating a larger network or adding more variables to the state vector for the networks.

As for recursive and online estimation of UAV parameters, recursive least squares (RLS) was carried out in [24] to identify a linear state-space model of a quadrotor, and in [25] to estimate its mass and inertia tensor while performing grasping missions. However, the off-diagonal elements of the inertia tensor were considered to be null when the rotation equation of the quadrotor was used to apply the regression. In [26], the Covariance Matrix Adaptation Evolution Strategy (CMA-ES) nonlinear identification approach was used to estimate the parameters of the nonlinear model of a coaxial micro helicopter. A Continuous-Time Identification Algorithm (CIA) was used in [27] to identify a quadrotor’s model dynamics for the motion along the vertical plane. The authors in [28] also made the symmetry assumption and used an Extended Kalman Filter (EKF) and an Unscented Kalman Filter (UKF) for the online estimation of the geometric and inertia parameters of a multi-rotor aerial vehicle. The proposed method also estimates the system’s center of mass position and its sensor module’s relative position. On the other hand, the moment of inertia estimates’ accuracy was relatively low, especially about the x - and z -axes where the average error was 19% and 9%, respectively. In [29], an adaptive control system and a gradient-type algorithm were used to identify in real-time the inertia tensor, mass, and wind parameters of a quadrotor mini-aircraft. Yet, only the estimation of the system’s changed mass was tested in simulation and experiment. An online adaptive parameter estimation was also developed in [30] to estimate the mass and the

diagonal elements of the moment of inertia tensor of a quadrotor. A scheme to obtain an expression of the estimation error was derived by introducing auxiliary filtered variables, and then an augmented matrix was constructed based on the derived filtered variables, which was further used to design the adaptive law to achieve convergence under the standard persistent excitation (PE) condition. However, the designed estimator was not validated by adding payloads to the quadrotor in simulation and experiment.

The main gap that exists in the literature of this topic is that when online estimation of the inertia tensor of quadrotors is implemented, it is assumed to be symmetric with null off-diagonal elements. This decreases the number of parameters in the estimation scheme and the identification becomes simpler, yet less accurate. Since the null off-diagonal elements assumption is not valid in real-life quadrotor systems, especially those intended for package delivery purposes where packages come in different sizes, shapes, and masses, the motion tracking performance of the quadrotor will be reduced. In this thesis, an identification scheme is proposed to estimate all nine elements of the 3x3 moment of inertia tensor matrix along with the system's total mass, which can be utilized to design adaptive control laws that can be employed in quality control systems for detecting payload characteristics and implemented in health monitoring algorithms. Yet, the dynamic parameters of a robot produce physical restrictions that should be addressed in the identification scheme. For instance, a quadrotor's mass is positive and its inertia matrix is symmetric and positive definite [31]; these conditions are represented by mathematical constraints to yield physically consistent estimates.

Chapter 3

System Modeling

3.1 Coordinate Frame:

Figure 3.1 represents the coordinates systems and the free body diagram of the quadrotor [32]. W is the world frame or inertial frame and B is the body-fixed frame attached to the center of mass. The world frame is used to express the position and the orientation vectors of the vehicle's center of mass which are $[x, y, z]^T$ and $[\phi, \theta, \psi]^T$ respectively. Then, the quadrotor presents six degrees of freedom, where ϕ , θ and ψ represents the roll, pitch and yaw movements respectively. $Z - X - Y$ Euler angles are used to model the rotation of the quadrotor in the world frame, the corresponding rotation matrices are, respectively:

$$R_1 = Rot(z, \psi) = \begin{bmatrix} c\psi & -s\psi & 0 \\ s\psi & c\psi & 0 \\ 0 & 0 & 1 \end{bmatrix} \quad (3.1)$$

$$R_2 = Rot(x, \phi) = \begin{bmatrix} 1 & 0 & 0 \\ 0 & c\phi & -s\phi \\ 0 & s\phi & c\phi \end{bmatrix} \quad (3.2)$$

$$R_3 = Rot(y, \theta) = \begin{bmatrix} c\theta & 0 & s\theta \\ 0 & 1 & 0 \\ -s\theta & 0 & c\theta \end{bmatrix} \quad (3.3)$$

Therefore, the rotation matrix that transforms the coordinates from B to W is:

$${}^W R_B = R_1 * R_2 * R_3 = \begin{bmatrix} c\psi c\theta - s\phi s\psi s\theta & -c\phi s\psi & c\psi s\theta + c\theta s\phi s\psi \\ c\theta s\psi + c\psi s\phi s\theta & c\phi c\psi & s\psi s\theta - c\psi c\theta s\phi \\ -c\phi s\theta & s\phi & c\phi c\theta \end{bmatrix}. \quad (3.4)$$

By denoting $[p, q, r]^T$ as the angular velocity vector in the body frame, it is calculated from the Euler rates vector using the following transformation matrix:

$$\begin{bmatrix} \dot{p} \\ \dot{q} \\ \dot{r} \end{bmatrix} = \begin{bmatrix} 0 \\ \dot{\theta} \\ 0 \end{bmatrix} + R_2^T \begin{bmatrix} \dot{\phi} \\ 0 \\ 0 \end{bmatrix} + R_3^T R_2^T \begin{bmatrix} 0 \\ 0 \\ \dot{\psi} \end{bmatrix}, \quad (3.5)$$

leading to:

$$\begin{bmatrix} \dot{p} \\ \dot{q} \\ \dot{r} \end{bmatrix} = \begin{bmatrix} c\theta & 0 & c\phi s\theta \\ 0 & 1 & s\phi \\ s\theta & 0 & c\phi c\theta \end{bmatrix} \begin{bmatrix} \dot{\phi} \\ \dot{\theta} \\ \dot{\psi} \end{bmatrix}, \quad (3.6)$$

where s and c are abbreviations of the sine and cosine functions, and R_2^T and R_3^T are the transpose matrices of R_2 and R_3 , respectively.

3.2 Rigid Body Dynamics:

The six degrees-of-freedom rigid-body equations of motion are derived by applying the Newton-Euler formalism in the world frame. The forces on the system are gravity and the thrust generated by each of the rotors F_i . Then, the linear acceleration of the center of mass is:

$$m \frac{dv}{dt} + w \times mv = F, \quad (3.7)$$

which becomes:

$$m \ddot{r} = \begin{bmatrix} 0 \\ 0 \\ -mg \end{bmatrix} + {}^W R_B \begin{bmatrix} 0 \\ 0 \\ \sum F_i \end{bmatrix}, \quad (3.8)$$

where r and v represent the position and velocity vectors in the world frame, respectively, m is the mass of the quadrotor, and g is the gravitational acceleration.

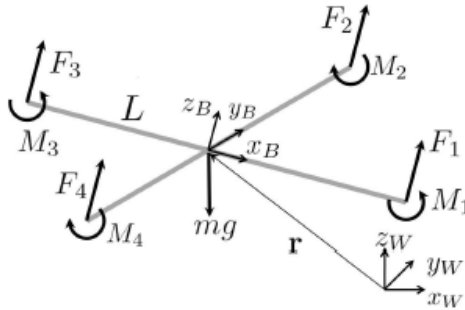


Figure 3.1: Quadrotor free body diagram

Rotors 1 and 3 rotate in the $-z_B$ direction, and since the moment produced on the quadrotor's chassis is opposite to the direction of rotation of the blades, then M_1 and M_3 are positive whereas M_2 and M_4 are negative. With L , the distance from the axis of rotation of the rotors to the center of the quadrotor, and using the Euler rotational equation of motion, the rotational acceleration is given by:

$$I \frac{dw}{dt} + w \times Iw = \tau, \quad (3.9)$$

which becomes:

$$I \begin{bmatrix} \dot{p} \\ \dot{q} \\ \dot{r} \end{bmatrix} = \begin{bmatrix} L(F_2 - F_4) \\ L(F_2 - F_4) \\ M_1 - M_2 + M_3 - M_4 \end{bmatrix} - \begin{bmatrix} p \\ q \\ r \end{bmatrix} \times \begin{bmatrix} p \\ q \\ r \end{bmatrix}, \quad (3.10)$$

where I is the inertia tensor that can be written as:

$$I = \begin{bmatrix} I_{xx} & I_{xy} & I_{xz} \\ I_{yx} & I_{yy} & I_{yz} \\ I_{zx} & I_{zy} & I_{zz} \end{bmatrix}. \quad (3.11)$$

The thrust force of each motor is given by:

$$F_i = c_T w_i^2 \quad (3.12)$$

where c_T is the thrust coefficient. Similarly, the drag torque is given by:

$$M_i = c_Q w_i^2, \quad (3.13)$$

where c_Q is the drag coefficient.

Thus, the total thrust and moments about the x -, y -, and z -axes can be written as:

$$\begin{bmatrix} \sum F \\ \tau_x \\ \tau_y \\ \tau_z \end{bmatrix} = \begin{bmatrix} c_T & c_T & c_T & c_T \\ 0 & Lc_T & 0 & -Lc_T \\ -Lc_T & 0 & Lc_T & 0 \\ c_Q & c_Q & c_Q & c_Q \end{bmatrix} \begin{bmatrix} w_1^2 \\ w_2^2 \\ w_3^2 \\ w_4^2 \end{bmatrix}. \quad (3.14)$$

The control system computes the needed thrust and moments and commands the speed of each motor to track a desired trajectory. The rotor speeds are given as reference for the Direct current (DC) motors whose dynamics are presented as a first-order system. The DC motor is a second order system, whose angular speed w_m is calculated from the applied voltage V using the following Laplace transform equation:

$$\frac{w_m(s)}{V(s)} = \frac{K_t}{(J s + b)(L s + R) + K_t K_e}, \quad (3.15)$$

where J is the moment of inertia of the rotor, b is the motor viscous friction constant, K_e is the electromotive force constant, K_t is the motor torque constant, R is the electric resistance, L is the electric inductance, and s is the Laplace operator. The mechanical dynamics are considered slow compared to the fast electrical dynamics. Thus, the slower pole will dominate the dynamics and the DC motor can be modeled then as a first order system up to a certain range of frequencies. Therefore, the transfer function relating the applied voltage, V , to the motor speed, w_m , is given by [33]:

$$\frac{w_m(s)}{V(s)} = \frac{K_m}{T_m s + 1}, \quad (3.16)$$

where K_m is the the Direct Current (DC) motor gain, and T_m is the motor's time constant.

Chapter 4

System Identification

System identification is defined as using observed input-output data to build mathematical models of dynamic systems. Yet, the generation of this data depends on the identification experiment [8]. When the system to be identified operates as part of a closed-loop configuration such as a quadrotor, several experimental approaches may be used to generate identification data. An evident approach is an open-loop experiment, where the controller feedback loop is opened and direct input signals are given to the system and output data is recorded. On the other hand, an alternative method can be conducted where the system is identified while it is executed in its closed-loop structure and disturbances are introduced via set point changes [34]. Figure 4.1 illustrates the open-loop and closed-loop configurations where u is the system input, y is the system output, r the reference or set point, C the controller, and G represents the system.

In fact, each method has its own advantages and disadvantages, thus multiple factors should be taken into account when deciding on the approach to be adopted. In open-loop, the user has total control on the direct input that is applied to the system, which allows for more control of the persistence of excitation (PE) conditions and generation of more informative data. However, controlling

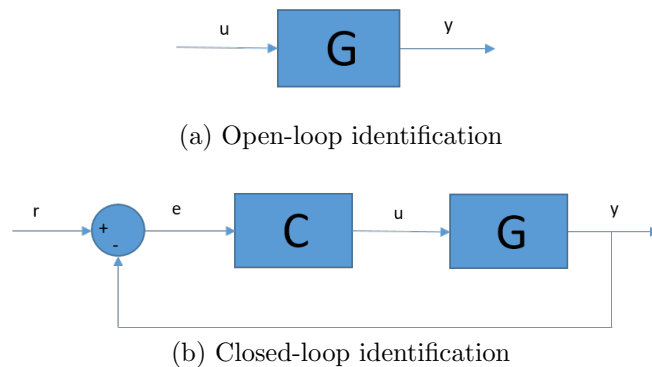


Figure 4.1: open-loop and closed-loop identification

an unstable system in open-loop may be detrimental for the system and its surroundings. Hence, it is more practical to operate it in closed-loop to reduce the influence of disturbances on the system, allow constrained output identification, and permit for better identification of control-relevant dynamics [35]. Nevertheless, the main drawback of closed-loop identification is that the feedback loop causes correlations between the input signals and the system noise leading for biasedness in the estimates. In addition, the rejection of disturbances leads to a reduction of the excitation level of the system and the information content in the data used for identification [36]. Due to the aforementioned issues of closed-loop estimation, and although they work well when adapted for open-loop data, most well-known identification methods such as correlation and spectral analysis methods fail when applied directly to input-output data captured from a closed-loop system [35, 36]. To tackle this challenge, Forsell & Ljung proposed the prediction error method (PEM) as a robust approach under closed-loop conditions as demonstrated in [37], which makes it suitable for a wide range of data conditions and parameterization structures. In addition, PEM has the ability to achieve minimum asymptotic variance that is comparable to that achieved under open-loop conditions [34][38].

When performing closed-loop system identification, three main approaches are available [35]:

1. Direct approach: feedback is ignored and the system is identified using only input-output data.
2. Indirect approach: the system is identified in closed-loop using the reference signal as the input; then based on the knowledge of the controller, the open-loop system is estimated.
3. Joint input-output (I/O) approach: the input is jointly regarded with the output as the output of the closed-loop system is driven by a certain reference subjected to noise. Then the open-loop system parameters along with the feedback signal are estimated.

It is noted that the indirect approach requires perfect knowledge of the controller, and the joint I/O approach requires at least the knowledge of the controller *structure*. Thus, the identification scheme can be very complex when applying these two approaches to a closed-loop system that is controlled by a nonlinear controller. On the other hand, the direct approach does not require any knowledge of the feedback control law structure or the controller type. Since many systems used for quadrotors motion control are nonlinear to achieve solid performance and account for nonlinearities, the direct approach is deemed as the most suitable approach and is adopted in this thesis. However, a main point to consider with the direct method is the risk that the closed-loop system may lose its identifiability in case of regulation, where no reference signal is applied, which should be taken into careful consideration to circumvent its occurrence [8].

4.1 Persistence of Excitation

The primary principle behind the success of any identification process is the choice of experimental conditions, which have a strong influence on the accuracy of the estimated model. In fact, the primary design variables are the signal input characteristics, the total experiment time, and the sampling rate [39]. These variables should be optimized to obtain the most informative data leading to the highest accuracy. The primary and most important variable is the input signal since it allows for the identifiability of the model structure that uniquely describes the data set. This is achievable, if and only if, the input is persistently excited to a sufficiently high order [8]. In closed-loop identification, the problem becomes more challenging since there is no direct access to the input signal making persistence of excitation (PE) hard to guarantee. Furthermore, even if PE conditions are attained, the system may not be identifiable when no reference signal is applied and the system performs regulation, thus the problem is solved by including a reference signal [8]. An input is persistently exciting of order n , if and only if, the rank of its covariance matrix is n , i.e. its power spectral density is larger than zero at n distinct frequencies. In summary, if the system contains n unknown parameters, the closed-loop control signal should be persistently exciting such that its spectral density is larger than zero at n distinct frequencies to excite all modes corresponding to the individual parameters.

4.2 Recursive Least Squares

In model-based control systems, having an accurate model is critical and that is especially true when the system properties vary over time, which is when online estimation is crucial to give the control system the ability to adapt and account for changes in order to maintain stability and tracking performance. In recursive identification methods, the parameter estimates are calculated recursively over time: if the parameter estimate is $\hat{\theta}_{t-1}$ at iteration $t - 1$, then recursive identification computes the new estimate $\hat{\theta}_t$ by updating $\hat{\theta}_{t-1}$ with a gain-multiplied error when a new observation becomes available at iteration t [40].

Several methods exist for recursive identification including recursive least squares (RLS), Kalman filter (KF), recursive instrumental variable (RIV), recursive maximum likelihood (RML), and extended least squares (ELS) [41, 42, 43]. A comparison between RLS, RIV, RML and ELS was conducted in [41], where it was stated that RLS provided the fastest convergence rate and the smallest computational effort and complexity. On the other hand, RLS estimates were poor (biased) compared to other algorithms when the signal-to-noise ratio is large. Furthermore, RLS does not estimate noise dynamics whereas RML and ELS exhibit this property. The same conclusion was reached in [39] and [43] in which RLS performance was compared to the Kalman filter in terms of computational

complexity and speed. In addition, it was shown that RLS does not require the knowledge of the covariance matrix of the noise, whereas Kalman filtering gives better estimates than RLS in terms of accuracy and biasedness.

Since the quadrotor model is unstable, fast estimation of the varying parameters needs to be performed. Furthermore, since the quadrotor's on-board processor consumes a majority of the computational power to execute feedback control, a lightweight algorithm in terms of computational effort and memory usage is required to perform the estimation. Given that, the recursive least squares method is employed in this work as the identification approach to estimate the quadrotor parameters. The adopted scheme is based on the prediction error method (PEM) [37], which aims at minimizing a cost function of the squared errors between measured outputs of the actual system and the predicted outputs of the estimated model, which is expressed as:

$$\hat{y} = \varphi^T \hat{\Theta}, \quad (4.1)$$

where φ is the regressor vector and $\hat{\Theta}$ is the parameters vector. The cost function to be minimized is given by:

$$V(\hat{\Theta}) = \|y - \hat{y}\|^2 = \sum_{k=1}^n \lambda^{n-k} (y[k] - \varphi[k] \hat{\Theta})^2, \quad (4.2)$$

where $\lambda \leq 1$ is a forgetting factor used to discount old data to cope with parameters changes, k is the current time step, and n is last time step. The cost function is solved recursively to yield the following recursive least squares (RLS) estimation algorithm with exponential forgetting [40]:

$$\begin{aligned} \epsilon[k] &= y[k] - \varphi^T[k] \hat{\Theta}[k-1], \\ P[k] &= \frac{1}{\lambda} \left(P[k-1] - \frac{P[k-1] \varphi[k] \varphi^T P[k-1]}{\lambda + \varphi^T[k] P[k-1] \varphi[k]} \right), \\ K[k] &= P[k] \varphi[k], \\ \hat{\Theta}[k] &= \hat{\Theta}[k-1] + K[k] \epsilon[k]. \end{aligned} \quad (4.3)$$

where ϵ is the error between the measured and the estimated output, P is the covariance matrix, K is the gain that multiplies the error to update the parameters and k is the current sample.

4.3 Covariance Resetting

In some applications, in which the physical properties of the system are changing, it is crucial to track the variations in its dynamics. To do so, it is indispensable to discount old data. However, this process involves compromises. If the parameters are constant, it is preferable to base the estimation on many measurements to

to reduce the effect of disturbances. On the other hand, if the system is changing, it can be very misleading to use a long data record since the parameters may be changing eventually. To accommodate this problem, the best solutions are obtained if the nature of the parameters variations is known. In fact, two prototype situations are presented: one case is when the parameters are slowly drifting, whereas the other case is when the parameters are constant for long periods, and then they jump from one value to another. The former is solved using exponential forgetting. As mentioned in the previous section, it is based on the assumption that the least-squares function is replaced by a loss function that exponentially discounts old data. Exponential forgetting works well when system parameters change homogeneously, however it is less effective in the face of occasional abrupt changes. When sudden parametric variations are expected, the covariance matrix is reset to a large value, which is known as covariance resetting (CR) [44]. To apply CR, the residual between the measured and the estimated outputs is continuously monitored, and when it exceeds a specified threshold, the covariance matrix is reset either by decreasing the forgetting factor to $\lambda = 0.0001$ or by resetting the covariance matrix elements directly. In case of a quadrotor system, when it picks up, carries, and drops off delivery packages, its mass and inertia tensor matrix changes abruptly. Therefore, it is substantial in this case to use covariance resetting to track these changes rapidly. This fast tracking ability helps the quadrotor's control system to promptly adapt to the system dynamical changes, which enables it to present an enhanced performance. To apply CR on the quadrotor, the sudden system variations can be firstly detected via tracking the total thrust generated by the motors to enable the quadrotor to hover in place. Once the variation is detected, the covariance matrix is reset to a defined value. This is done by performing the following alteration on the RLS algorithm shown in eq. (4.3)

$$\begin{aligned}
\epsilon[k] &= y[k] - \varphi^T[k]\hat{\Theta}[k-1], \\
\text{if variation=true: } P[k] &= \text{diag}(np) * Val \\
\text{else: } P[k] &= \frac{1}{\lambda} \left(P[k-1] - \frac{P[k-1]\varphi[k]\varphi^T P[k-1]}{\lambda + \varphi^T[k]P[k-1]\varphi[k]} \right), \\
K[k] &= P[k]\varphi[k], \\
\hat{\Theta}[k] &= \hat{\Theta}[k-1] + K[k]\epsilon[k],
\end{aligned} \tag{4.4}$$

where np is the number of parameters that need to be estimated, $\text{diag}(np)$ is an $np \times np$ diagonal matrix and Val is the value of its diagonal elements.

4.4 Physical feasibility of inertial parameters identification

Dynamic parameters of robots have a physical meaning, thus the physical feasibility of the obtained values should be taken into consideration when they are estimated [31]. In fact, when parameter estimation is performed using linear equations that model nonlinear systems, the physical feasibility of the estimated values may not be guaranteed. In this work, since the inverse of the inertia matrix is estimated first and then the latter is calculated by inversion as it will be shown later, the physical consistency of the identified values is critical. In particular, if the obtained values of the inertia matrix inverse are not physically feasible, it will not be invertible, and hence the inertia tensor could not be calculated.

Physical consistency of quadrotor dynamic parameters as defined by [45] is described by the following conditions:

$$\begin{cases} m > 0 \\ I \succ 0, \end{cases} \quad (4.5)$$

where m is the system mass, I is its inertia matrix, and $\succ 0$ denotes positive definiteness of I . This means that its inverse, $J = I^{-1}$, is also positive definite:

$$J \succ 0, \quad (4.6)$$

thus it can be diagonalised and written as:

$$J = R G R^T, \quad (4.7)$$

where G is a 3x3 diagonal matrix whose elements are the eigenvalues of J :

$$G = \begin{bmatrix} G_x & 0 & 0 \\ 0 & G_y & 0 \\ 0 & 0 & G_z \end{bmatrix}, \quad (4.8)$$

and R is a 3x3 orthogonal rotation matrix that aligns the reference frame with the principal axes of rotation. Since I is calculated using a set of integrals over the body mass density, its eigenvalues and equivalently the eigenvalues of its inverse are always positive guaranteeing that $I \succ 0$, then

$$\begin{cases} G_x > 0, \\ G_y > 0, \\ G_z > 0. \end{cases} \quad (4.9)$$

However, the above condition is not sufficient to guarantee physical feasibility of the identified parameters [46]. Due to the positiveness of mass density, the

triangle inequality condition should be met. The condition states that the sum of any two eigenvalues is always greater than the remaining one:

$$\begin{cases} G_x + G_y > G_z, \\ G_y + G_z > G_x, \\ G_z + G_x > G_y, \end{cases} \quad (4.10)$$

Therefore, a 3x3 inertia matrix inverse is said to be physically feasible if it is symmetric, positive definite and, its eigenvalues satisfy the triangle inequality conditions [47]. Equation (4.10) can be written as:

$$\begin{cases} G_x + G_y + G_z > 2G_z, \\ G_y + G_z + G_x > 2G_x, \\ G_z + G_x + G_y > 2G_y, \end{cases} \quad (4.11)$$

which leads to:

$$\frac{G_x + G_y + G_z}{2} > \max(G_x, G_y, G_z). \quad (4.12)$$

Equation (4.12) can be reformulated as:

$$\frac{\text{trace}(I^{-1})}{2} > \lambda_{\max}(I^{-1}), \quad (4.13)$$

where λ_{\max} represents the maximum eigenvalue. If equation (4.13) is written in a matrix form, the resulted equation is:

$$\frac{\text{trace}(I^{-1})}{2} I_d \succ I^{-1}, \quad (4.14)$$

where I_d is a 3x3 identity matrix. Finally, equation (4.14) is expressed as:

$$Y = \frac{\text{trace}(I^{-1})}{2} I_d - I^{-1} \succ 0. \quad (4.15)$$

Chapter 5

Experimental Implementation

The proposed estimation scheme is first implemented on a three degrees-of-freedom (3 DOF) Hover platform that possesses roll, pitch, and yaw motions but without vertical take-off and landing (VTOL) capability. Once the scheme is validated on the 3 DOF Hover platform, it is then implemented on a real-life quadrotor system, the Quanser QBall-2 platform.

5.1 3 DOF Hover

Since directly running experiments on a quadrotor aerial vehicle can be challenging, and for safety reasons and platform preservation, it is decided to first run experiments and test the proposed algorithms on a “quadrotor-like” three degrees-of-freedom hover platform (3 DOF Hover) from Quanser. As shown in Fig. 5.1, it is a quadrotor that can only perform rotational movements, making it safer to use, more stable, and more suitable for indoor experimental testing.

Since the 3 DOF Hover platform does not move in the z -direction, (3.7) does not apply to its dynamics, which deems the identification of the mass impossible and only the moment of inertia can be estimated. The Euler angle velocities are the same as those of the body frame and (3.9) could be written as:

$$\begin{bmatrix} \ddot{\phi} \\ \ddot{\theta} \\ \ddot{\psi} \end{bmatrix} = [I^{-1}] \begin{bmatrix} 0 & \dot{\psi} & -\dot{\theta} \\ -\dot{\psi} & 0 & -\dot{\phi} \\ \dot{\theta} & -\dot{\phi} & 0 \end{bmatrix} [I] \begin{bmatrix} \dot{\phi} \\ \dot{\theta} \\ \dot{\psi} \end{bmatrix} + [I^{-1}] \begin{bmatrix} \tau_x \\ \tau_y \\ \tau_z \end{bmatrix}. \quad (5.1)$$

The nonlinear model in (5.1) is used to build a high fidelity simulation of the 3 DOF Hover in the MATLAB/Simulink environment to validate the identification scheme before its experimental implementation. When operating the platform around the zero Euler angles equilibrium point, the second term in the right hand of (5.1) can be neglected. The linearized input-output equation becomes:



Figure 5.1: Quanser 3 DOF Hover

$$\begin{bmatrix} \ddot{\phi} \\ \ddot{\theta} \\ \ddot{\psi} \end{bmatrix} = I^{-1} \begin{bmatrix} \tau_x \\ \tau_y \\ \tau_z \end{bmatrix}, \quad (5.2)$$

where τ_x , τ_y , and τ_z are the torques applied on the x -, y - and z - axes, respectively.

The direct identification approach can now be applied to each row of (5.2) with the unknown parameters being those of the inertia matrix inverse. For instance, by expressing $I^{-1} = J$ as:

$$J = \begin{bmatrix} A_{11} & A_{12} & A_{13} \\ A_{21} & A_{22} & A_{23} \\ A_{31} & A_{32} & A_{33} \end{bmatrix}, \quad (5.3)$$

the linear equations, on which linear regression is applied, are given by:

$$\begin{aligned} \ddot{\phi} &= A_{11} * \tau_x + A_{12} * \tau_y + A_{13} * \tau_z, \\ \ddot{\theta} &= A_{21} * \tau_x + A_{22} * \tau_y + A_{23} * \tau_z, \\ \ddot{\psi} &= A_{31} * \tau_x + A_{32} * \tau_y + A_{33} * \tau_z, \end{aligned} \quad (5.4)$$

where the $\ddot{\phi}$, $\ddot{\theta}$, and $\ddot{\psi}$ accelerations calculated by double differentiation of the measured Euler angles are considered the outputs of the linear regression model and the torques are the inputs or regressors. Thus, after estimating the parameters of J , the inertia matrix is obtained by matrix inversion operation. The corresponding RLS estimation algorithm with exponential forgetting on the roll dynamics equation is then given by:

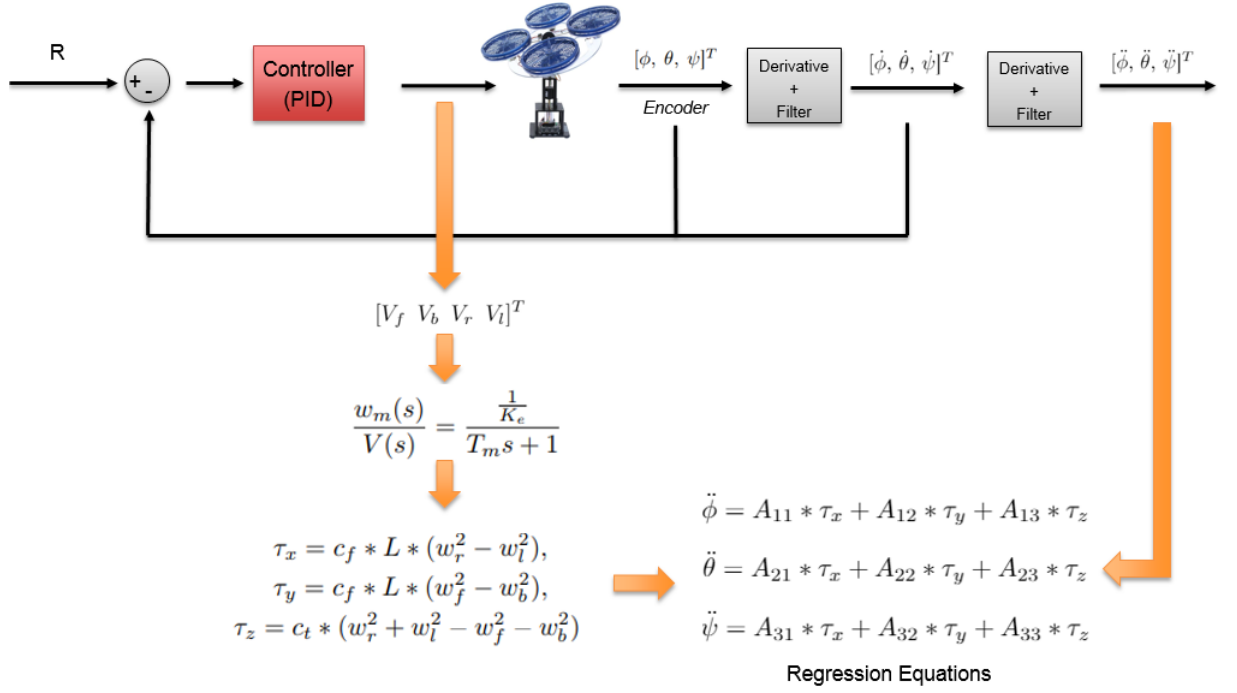


Figure 5.2: 3 DOF Hover's direct closed-loop identification scheme

$$\begin{aligned}
 \epsilon[k] &= \ddot{\phi}[k] - [\tau_x[k] \ \tau_y[k] \ \tau_z[k]] \begin{bmatrix} A_{11}[k-1] \\ A_{12}[k-1] \\ A_{13}[k-1] \end{bmatrix}, \\
 P[k] &= \frac{1}{\lambda} \left(P[k-1] - \frac{P[k-1] \varphi[k] \varphi^T P[k-1]}{\lambda + \varphi^T[k] P[k-1] \varphi[k]} \right), \\
 K[k] &= P[k] \begin{bmatrix} \tau_x[k] \\ \tau_y[k] \\ \tau_z[k] \end{bmatrix}, \\
 \begin{bmatrix} A_{11}[k] \\ A_{12}[k] \\ A_{13}[k] \end{bmatrix} &= \begin{bmatrix} A_{11}[k-1] \\ A_{12}[k-1] \\ A_{13}[k-1] \end{bmatrix} + K[k] \epsilon[k].
 \end{aligned} \tag{5.5}$$



Figure 5.3: Infrared obstacle sensor module (RKI-3141)

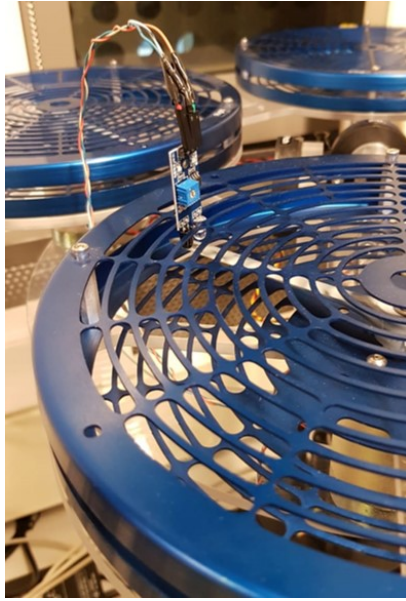


Figure 5.4: Infrared obstacle sensor mounted on the hover platform

Similarly, the RLS estimation algorithm that is applied on the pitch motion equation is given by:

$$\begin{aligned}
 \epsilon[k] &= \ddot{\theta}[k] - [\tau_x[k] \ \tau_y[k] \ \tau_z[k]] \begin{bmatrix} A_{21}[k-1] \\ A_{22}[k-1] \\ A_{23}[k-1] \end{bmatrix}, \\
 P[k] &= \frac{1}{\lambda} \left(P[k-1] - \frac{P[k-1]\varphi[k]\varphi^T P[k-1]}{\lambda + \varphi^T[k]P[k-1]\varphi[k]} \right), \\
 K[k] &= P[k] \begin{bmatrix} \tau_x[k] \\ \tau_y[k] \\ \tau_z[k] \end{bmatrix}, \\
 \begin{bmatrix} A_{21}[k] \\ A_{22}[k] \\ A_{23}[k] \end{bmatrix} &= \begin{bmatrix} A_{21}[k-1] \\ A_{22}[k-1] \\ A_{23}[k-1] \end{bmatrix} + K[k]\epsilon[k].
 \end{aligned} \tag{5.6}$$

Finally, the RLS estimation algorithm that is applied on the yaw motion equation is given by:

$$\begin{aligned}
\epsilon[k] &= \ddot{\psi}[k] - [\tau_x[k] \ \tau_y[k] \ \tau_z[k]] \begin{bmatrix} A_{31}[k-1] \\ A_{32}[k-1] \\ A_{33}[k-1] \end{bmatrix}, \\
P[k] &= \frac{1}{\lambda} \left(P[k-1] - \frac{P[k-1]\varphi[k]\varphi^T P[k-1]}{\lambda + \varphi^T[k]P[k-1]\varphi[k]} \right), \\
K[k] &= P[k] \begin{bmatrix} \tau_x[k] \\ \tau_y[k] \\ \tau_z[k] \end{bmatrix}, \\
\begin{bmatrix} A_{31}[k] \\ A_{32}[k] \\ A_{33}[k] \end{bmatrix} &= \begin{bmatrix} A_{31}[k-1] \\ A_{32}[k-1] \\ A_{33}[k-1] \end{bmatrix} + K[k]\epsilon[k].
\end{aligned} \tag{5.7}$$

To obtain accurate estimates of the inertia tensor elements, the measured accelerations (outputs) and the torques (inputs) should be as close as possible to the real accelerations and torques applied on the 3 DOF Hover platform. Thus, when recording encoder measurements (position) and differentiating twice to obtain acceleration signals, low-pass filters are used to attenuate high frequency noise content. As a result of the introduced low-pass filters, a time delay is induced in the outputs, which necessitates synchronizing the input signals before performing estimation. Furthermore, it is substantial that the model used to calculate the torques from the voltages sent to the 3 DOF Hover's motors, along with the identified parameters, represent the real system with high fidelity. In fact, the torques applied on the 3 DOF Hover air-frame are expressed as:

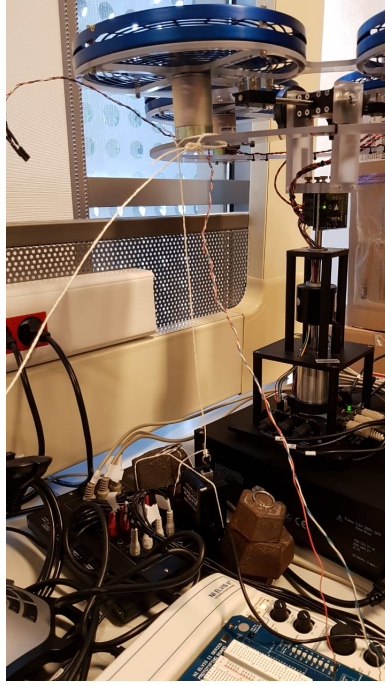


Figure 5.5: Vernier double range force sensor used for c_f identification

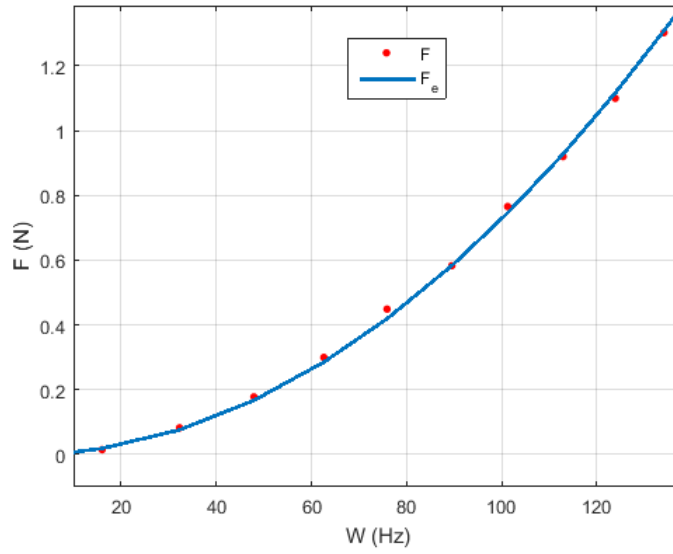


Figure 5.6: Identification of thrust coefficient c_f

$$\begin{aligned}
 \tau_x &= c_f * L * (w_r^2 - w_l^2), \\
 \tau_y &= c_f * L * (w_f^2 - w_b^2), \\
 \tau_z &= c_t * (w_r^2 + w_l^2 - w_f^2 - w_b^2),
 \end{aligned} \tag{5.8}$$

where τ_x , τ_y , and τ_z are the input torques, L is the hover's arm length, c_f is the thrust coefficient, c_t is the drag coefficient, and w_i is the angular speed of each motor.

While L is fixed and given, c_f and c_t need to be identified from measurements. Since the rotor angular velocities are not measured due to the absence of an on-board tachometer, they are estimated using the DC motor dynamic equation (3.16). The propellers blades attached to the motors induce aerodynamic drag forces, which tend to decrease the static gain and increase the time constant. Since the torques calculated in (5.8) are directly proportional to the accelerations, as demonstrated in (5.2), they are filtered by the same low-pass filters applied on the output to synchronize the two signals. Due to its simplicity, robustness, and disturbance rejection ability, a proportional-integral-derivative (PID) controller is used to control the 3 DOF Hover motion and generate the input commands to the system [48]. The identification scheme is portrayed in Fig. 5.2, where R is the reference signal.

The proposed estimation method is first tested in simulation for primary validation purposes. To implement the nonlinear model of the 3 DOF Hover represented by (3.9), the thrust and drag coefficients, c_f and c_t , and the DC motor characteristics are required to calculate the input torques. To accurately estimate the first-order model of the DC motors in (3.16), an infrared obstacle sensor module (RKI-3141), shown in Fig. 5.3, is used to determine the motor speed.

The sensor is mounted on the 3 DOF Hover platform as shown in Fig. 5.4. The sensor is high (1) when no obstacle is detected and low (0) when a propeller blade passes in front of it. Thus, each turn, the sensor output will be zero twice due to the presence of the two blades of the propeller. The speed is determined by measuring the frequency of the falling edges of the sensor output signal divided by two. The rise time is calculated by detecting the time needed for the rotational speed to reach 63% of its steady state value, which is the time constant of first-order systems.

After applying several input voltages, it is noted that the static gain depends on the applied voltage level, whereas the time constant is fixed. Thus, the first-order model of the DC motors is given by:

$$\frac{w_m(s)}{V(s)} = \frac{K_m}{0.2s + 1}, \quad (5.9)$$

with

$$K_m = -0.003008 u^2 - 0.01199 u + 8.072, \quad (5.10)$$

where u is the analogue voltage (between 0 and 24 V) applied on the motor.

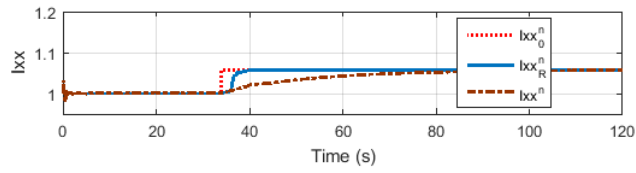
The inertia tensor of the Quanser 3 DOF Hover, as expressed in its data-sheet [1], are $I_{xx} = 0.0552$, $I_{yy} = 0.0552$, and $I_{zz} = 0.1104$, all in $kg - m^2$, and zero off-diagonal elements due to symmetricity assumption. Thrust coefficient, c_f , is identified by measuring the propeller's thrust force versus speed, and curve fitting the data in accordance with (3.12), as shown in Fig. 5.6, where F is the measured force and F_e is its estimate after identification. A dual range force sensor (Vernier DFS-BTA) is used to measure the force as shown in Fig. 5.5. Coefficient c_t is estimated beforehand by applying a square wave with frequency $f = 0.5 Hz$ and amplitude $A = 5^\circ$ to the 3 DOF Hover in the yaw degree-of-freedom, and using its corresponding linear regression equation (5.4), which becomes with $L = 0.1968 m$:

$$\ddot{\psi} = \frac{c_t}{0.1104} * (w_r^2 + w_l^2 - w_f^2 - w_b^2). \quad (5.11)$$

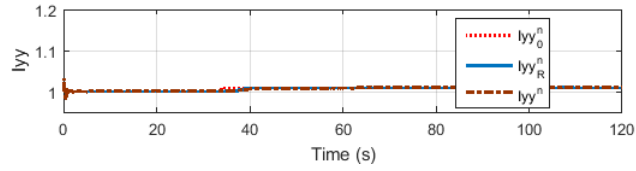
The final identification yields the following values: $c_f = 7.32 * 10^{-5} N$ and $c_t = 3.46 * 10^{-6} Nm$.

5.1.1 Simulation Results on the 3 DOF Hover

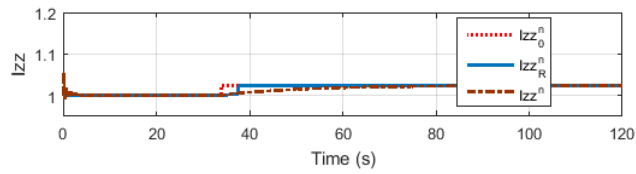
Since only the diagonal elements of the Quanser 3 DOF Hover's inertia matrix are given, they can be used as a reference to test the adequacy and accuracy of the estimation method. In fact, by getting accurate diagonal elements estimates, it can be deduced that the input torques are persistently exciting. This also indicates that the off-diagonal elements estimates are also accurate since they are estimated using the same inputs. Thus, in simulation and experimentation, the effect of mass addition on the inertia is studied on the diagonal elements only. The parallel axis theorem [49] is used to compute the effects of adding a cylindrical mass of $0.05 Kg$ under the left motor at time $t = 30 s$. For instance, the new inertia of the 3 DOF Hover about the x -axis is calculated as:



(a) Estimated parameter I_{xx} (normalized)

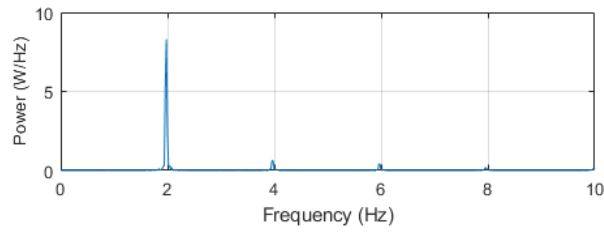


(b) Estimated parameter I_{yy} (normalized)

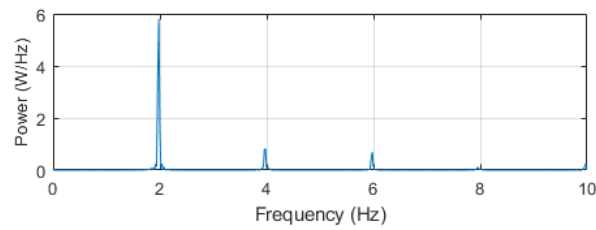


(c) Estimated parameter I_{zz} (normalized)

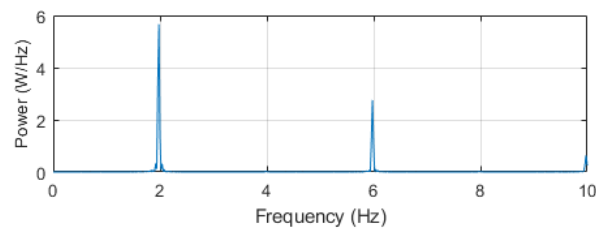
Figure 5.7: Estimates of the inertia tensor diagonal elements, in simulation, with and without covariance resetting.



(a) PSD of τ_x



(b) PSD of τ_y



(c) PSD of τ_z

Figure 5.8: Power spectral densities (PSD) of the input torques in simulation

$$\begin{aligned}
I_{xx_m} &= \frac{1}{12}M(3r^2 + h^2), \\
I_{xx_m}^{CG} &= I_{xx_m} + M(y^2 + z^2 + 2yz\sin(\phi)), \\
I_{xx_{new}} &= I_{xx_0} + I_{xx_m}^{CG},
\end{aligned} \tag{5.12}$$

where I_{xx_0} is the initial inertia of the 3 DOF Hover before the mass addition, M is the mass of a cylinder, r is its radius, h is its height, and y and z are the coordinates of the added mass when the platform is in its hovering position. The theoretical inertia matrix of the loaded system, with its off-diagonal elements manually set for testing, is given by:

$$I_{theoretical} = \begin{bmatrix} 0.05837 & 0.001 & 0.002 \\ 0.001 & 0.05573 & 0.003 \\ 0.002 & 0.003 & 0.1131 \end{bmatrix}.$$

The obtained matrix by the estimation algorithm at the end of the simulation is:

$$I_{estimated} = \begin{bmatrix} 0.05835 & 0.001291 & 0.001995 \\ 0.001291 & 0.05571 & 0.00301 \\ 0.001995 & 0.00301 & 0.1132 \end{bmatrix}.$$

For clarity purposes and due to their small values, the *normalized* estimates of diagonal elements I_{xx} , I_{yy} , and I_{zz} are shown in Fig. 5.7, with and without covariance resetting. $I_{xx_0}^n$ represents the theoretical value of I_{xx} , $I_{xx_R}^n$ represents its estimate *with* CR, and I_{xx}^n represents its estimate *without* CR. In comparison, both methods result in accurate estimates of I_{xx} , I_{yy} , and I_{zz} , but CR tends to increase the convergence rate, which is advantageous for prompt updates of the controller gains.

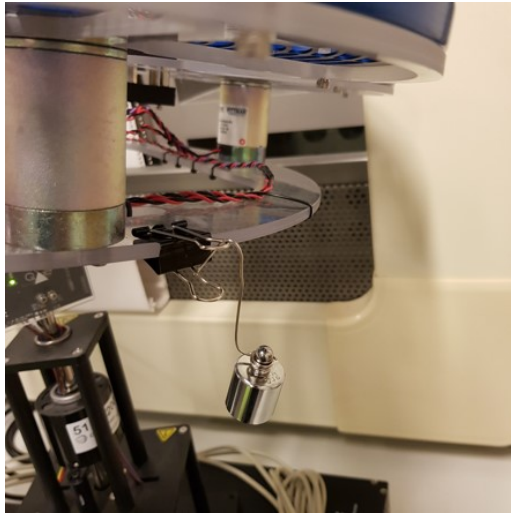
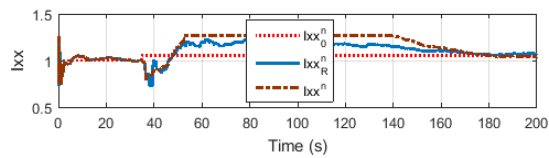
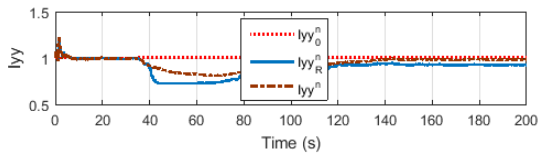


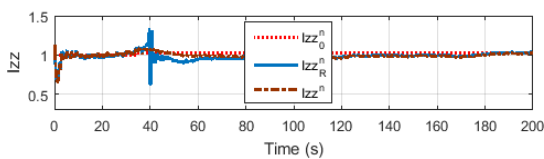
Figure 5.9: Added mass to the hover platform



(a) Estimated normalized parameter I_{xx}



(b) Estimated normalized parameter I_{yy}



(c) Estimated normalized parameter I_{zz}

Figure 5.10: Estimates of the inertia tensor diagonal elements, in experiment, with and without covariance resetting

Figure 5.8 shows the plots of the right side of the power spectral densities (PSD) of the input torques, which give an indication about their persistent excitation. As shown, τ_x and τ_y are PE with an order of at least 2, and τ_z is PE of order at least 4, which indicates that the input torques that are used in the linear regression equations are persistently exciting, thus yielding the accurate estimates shown in Fig. 5.7.

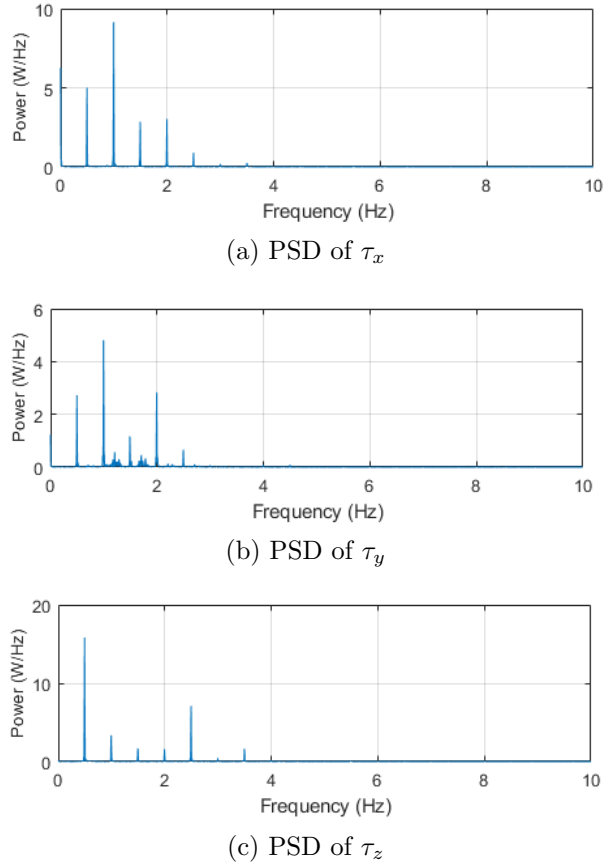


Figure 5.11: Power spectral densities (PSD) of the input torques in experiment

5.1.2 Experimental Validation

The identification scheme is experimentally validated through the addition of a $0.05Kg$ mass, by hanging it on the Quanser 3 DOF Hover frame underneath its left motor, at time $t = 30s$ into the experiment as shown in Fig. 5.9. The result of the identification is shown in Fig. 5.10. It is noted that the experiment has high frequency noise due to sensor measurements as opposed to simulation, thus the torque inputs are more persistently exciting, as shown by their PSDs in Fig. 5.11.

The obtained estimates are accurate, which validates the design of the proposed identification scheme, however, the convergence rate is deemed slow. I_{xx} estimation shows how covariance resetting boosts its convergence rate, whereas the estimation of I_{yy} presents a bias from the desired value. On the other hand, the I_{zz} estimation is not affected by covariance resetting except when the mass is added.

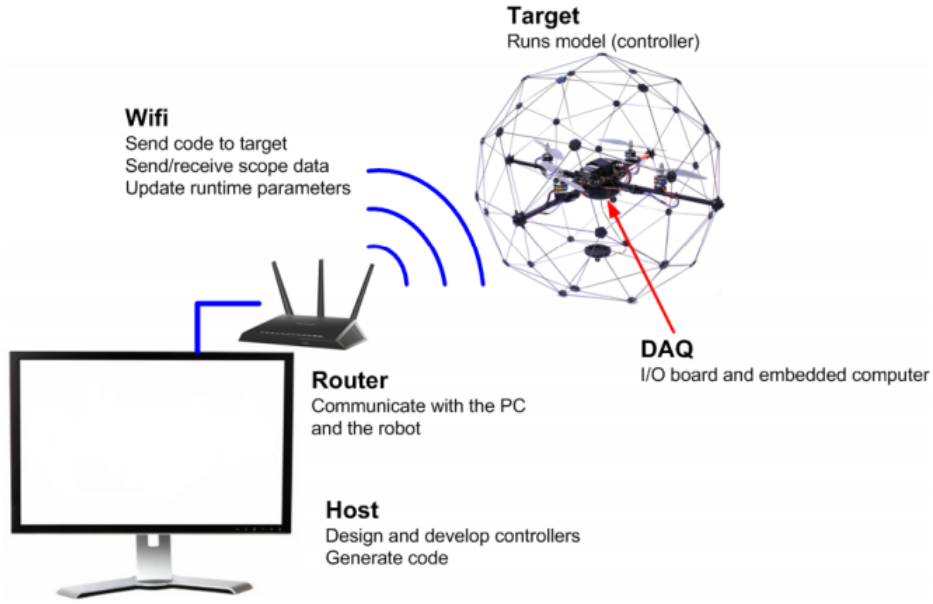


Figure 5.12: Qball2 quadrotor's command system [1]

5.2 QBall-2 Quadrotor

After validating the inertia tensor estimation methodology on the 3 DOF Hover platform, it is implemented and validated on a real quadrotor. In addition to the inertia estimation, it is required to estimate the varying mass of the quadrotor when it carries a payload. In this work, the Quanser QBall-2 quadrotor is used to carry a payload and to estimate its changing mass and inertia tensor. The QBall-2 quadrotor, shown in Fig. 5.12, is an indoor rotary wing platform that is operated using a ground station and using OptiTrack cameras. It is propelled by four Park 480 Brushless motors - 1020Kv fitted with 10x4.7 inch APC propellers. The entire quadrotor is enclosed within a protective carbon fiber cage, which ensures safe indoor operation. To read measurements from on-board sensors and drive the propeller motors, the QBall-2 utilizes an on-board avionics data acquisition card (DAQ) and a wireless Gumstix DuoVero embedded computer [50]. The quadrotor's mass is $M = 1.73Kg$ and its arms length is $L = 0.2m$. The moments of inertia matrix used in the nonlinear model (3.9) is considered diagonal with values: $I_{xx_0} = I_{yy_0} = 0.03Kg.m^2$ and $I_{zz_0} = 0.04Kg.m^2$.

The OptiTrack Motion Capture System is operated by the ground station and tracks the position and orientation of the QBall-2 and sends it to the quadrotor's embedded system via WiFi. The interface to the QBall-2 is MATLAB/Simulink with QUARC library. The controllers are developed in Simulink with QUARC on the host computer, and these models are downloaded and compiled into executables on the target, which in return sends the real-time data to the ground station. A diagram of this configuration is shown in Fig. 5.12.

The same estimation used on the 3 DOF Hover platform is used on the Qball-2 quadrotor, however, the input torques and the output accelerations in the linear regression equations (5.4) are measured differently. In fact, to model the Qball-2, Quanser identifies the DC motors as the following normalized first-order transfer function:

$$\frac{w_i(s)}{u(s)} = \frac{1}{0.066s + 1}, \quad (5.13)$$

where w_i is the normalized rotational speed of the motor i ; $i = \{b, f, l, r\}$ represents the back, front, left, and right motors, respectively; and u is the voltage (between 0 and 1) sent to the motors electronic speed controller (ESC). Quanser also identifies the maximum thrust and drag torque generated by each motor as $K = 12 \text{ N}$ and $Ky = 0.4 \text{ Nm}$, respectively. Therefore, the torques are calculated by:

$$\begin{aligned} \tau_x &= K * L * (w_l^2 - w_r^2), \\ \tau_y &= K * L * (w_b^2 - w_f^2), \\ \tau_z &= Ky * (w_r^2 + w_l^2 - w_f^2 - w_b^2), \end{aligned} \quad (5.14)$$

where L is the quadrotor's arm length. However, since the QBall-2 uses Lithium-ion batteries, their voltages is not constant over time, hence the battery drain effect should be included to improve the identification process. The battery drain model used in experiment is a simple linear interpolation between two corresponding battery voltages to two weighing factors multiplying the thrust created by each motor calculated using (3.12), as illustrated in Fig. 5.13. The torques are calculated by:

$$\begin{aligned} \tau_x &= bd * K * L * (w_l^2 - w_r^2), \\ \tau_y &= bd * K * L * (w_b^2 - w_f^2), \\ \tau_z &= bd * Ky * (w_r^2 + w_l^2 - w_f^2 - w_b^2), \end{aligned} \quad (5.15)$$

where bd is the battery drain model factor calculated at each time step depending on the battery voltage. As for the angular accelerations, an STMicroelectronics 3-axis gyroscope [51] is used to estimate the roll, pitch, and yaw angular speeds, and then by applying differentiation and appropriate filtration, the angular accelerations are calculated. A PID controller is used to control the quadrotor motion and to generate the input commands to the system. The identification scheme is portrayed in Fig. 5.14.

As for the mass estimation, equation (3.7) for the motion in the z -axis is used, which is expressed as follows:

$$m\ddot{z} = F_T \cos\phi \cos\theta - mg, \quad (5.16)$$

where $F_T = K(w_b^2 + w_f^2 + w_l^2 + w_r^2)$ is the total force generated by the motors. By operating the quadrotor in a hovering state, the derivatives of the position

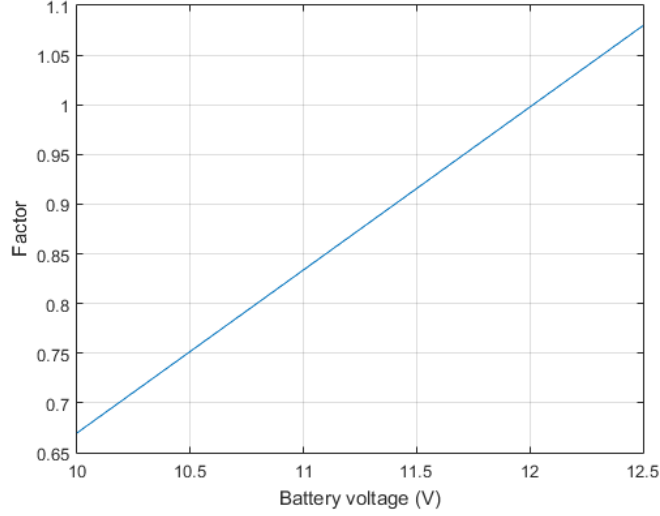


Figure 5.13: Battery drain effect model

and Euler angles states are zero. Furthermore, the roll and pitch angles are approximately negligible. Thus, the linearized version of equation (5.16) becomes:

$$g = \frac{1}{m} F_T, \quad (5.17)$$

which is the regression equation on which the RLS algorithm is applied to estimate the mass where g is the output and F_T is the input.

The RLS algorithm for the mass estimation is then:

$$\begin{aligned} \epsilon[k] &= g[k] - F_T[k] m_{inv}[k-1], \\ P[k] &= \frac{1}{\lambda} \left(P[k-1] - \frac{P[k-1] \varphi[k] \varphi^T P[k-1]}{\lambda + \varphi^T[k] P[k-1] \varphi[k]} \right), \\ K[k] &= P[k] [m_{inv}[k]], \\ [m_{inv}[k]] &= [m_{inv}[k-1]] + K[k] \epsilon[k]. \end{aligned} \quad (5.18)$$

5.2.1 Simulation Results

To validate the estimation scheme of the varying mass and inertia tensor of a quadrotor system, it is firstly implemented in simulation. The nonlinear model represented by equation (3.9) is used and the torques are calculated from the controller's output voltages using equations (5.13) and (5.14).

First, the quadrotor is commanded to perform oscillatory movements around its axes by sending sinusoidal desired trajectories to its Euler angles. This achieves a persistently exciting input that enables the estimated parameters to be accurate and unbiased. A mass of $0.1Kg$ is added at time $t = 15s$ at coordinates $r_x = 0.25m$, $r_y = 0.15m$, and $r_z = -0.05m$, and it is removed at time $t = 35s$.

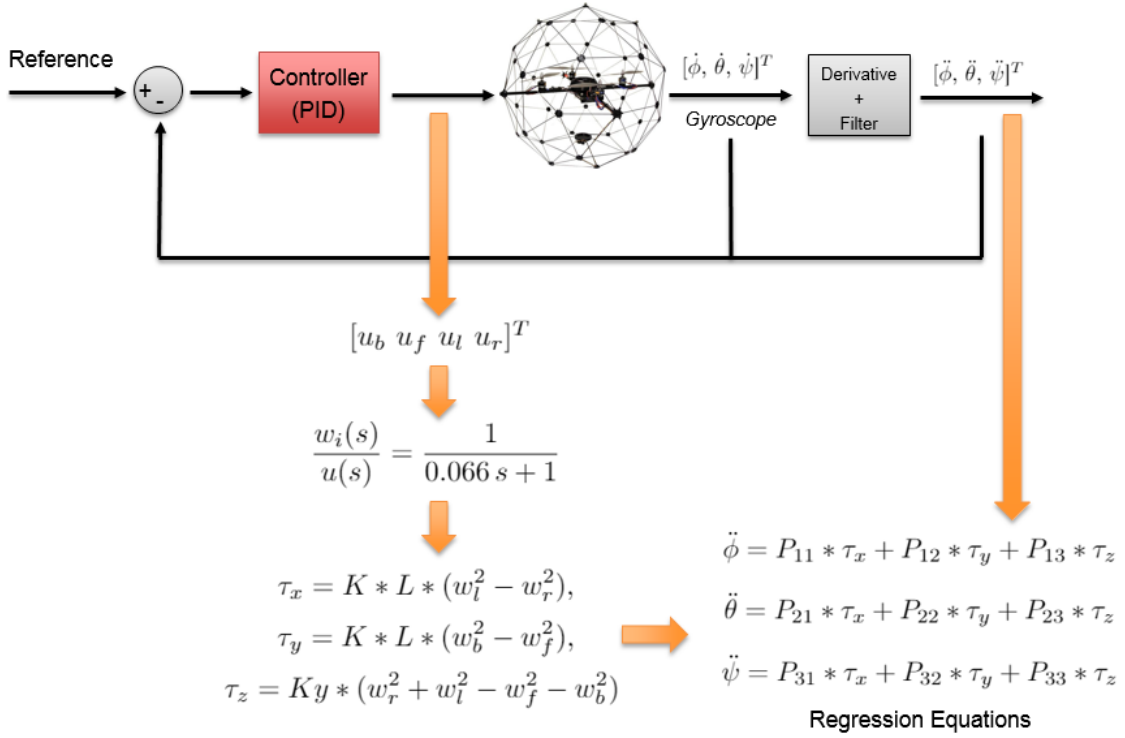


Figure 5.14: QBall-2 inertia tensor identification scheme.

To estimate the mass, a forgetting factor, $\lambda_m = 0.999$, is used and the result is shown in Fig. 5.15, where m_d is the desired mass and m is its estimate.

When the mass is added, it creates two torques about the x - and y -axes. The values of these resultant torques are, respectively:

$$\begin{aligned}
 \tau_{mx} &= -r_y * m_{add} * g, \\
 \tau_{my} &= r_x * m_{add} * g,
 \end{aligned}
 \tag{5.19}$$

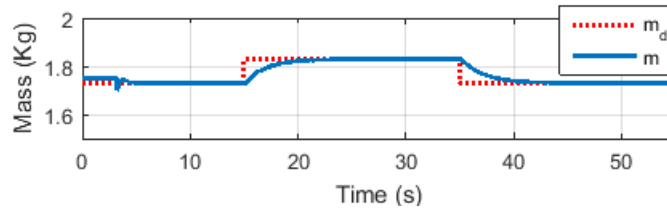


Figure 5.15: Quadrotor's mass estimation in numerical simulation

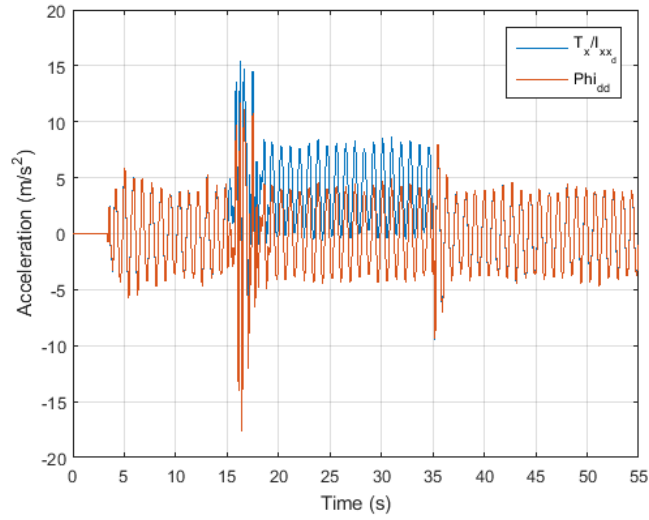


Figure 5.16: Non filtered torque Vs. roll measured acceleration in simulation

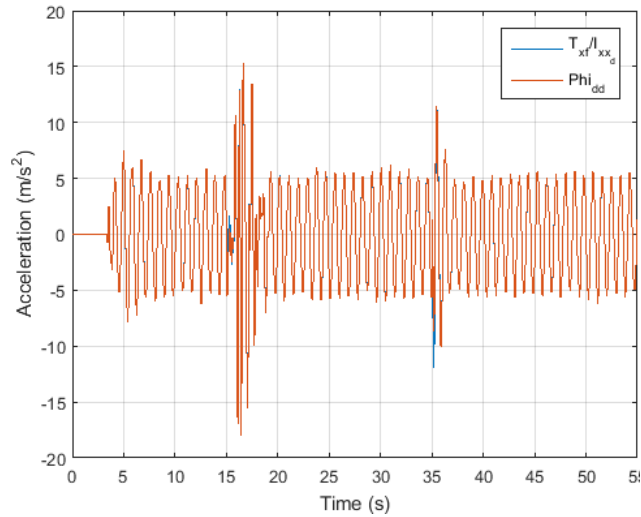


Figure 5.17: Filtered torque Vs. roll measured acceleration in simulation

where m_{add} is the value of the added mass. Thus, to provide the same output performance as that provided before the mass addition, the control system in-

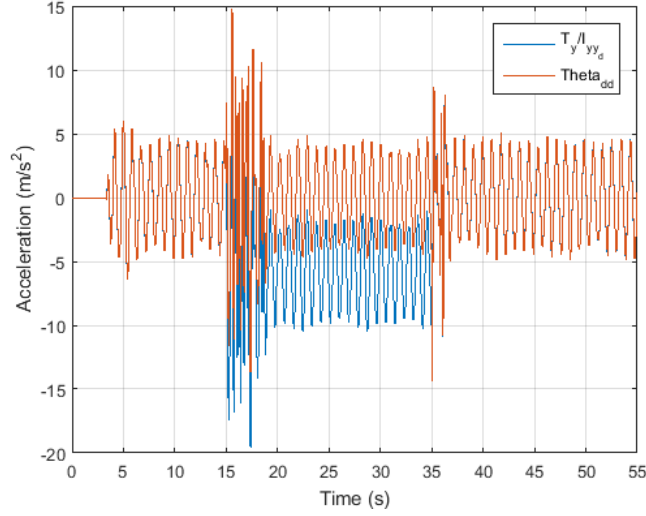


Figure 5.18: Non filtered torque Vs. pitch measured acceleration in simulation

creates the input torques with offsets equal to τ_{mx} and τ_{my} . The new system's rotational equations of motion are then:

$$\begin{aligned}\ddot{\phi} &= A_{11} * \tau_x + A_{12} * \tau_y + A_{13} * \tau_z + \tau_{mx}, \\ \ddot{\theta} &= A_{21} * \tau_x + A_{22} * \tau_y + A_{23} * \tau_z + \tau_{my}, \\ \ddot{\psi} &= A_{31} * \tau_x + A_{32} * \tau_y + A_{33} * \tau_z.\end{aligned}\tag{5.20}$$

High-pass filters are used to remove the mentioned offsets from the input torques. Thus, the final regression equation is given by:

$$\begin{aligned}\ddot{\phi} &= A_{11} * \tau_{xf} + A_{12} * \tau_{yf} + A_{13} * \tau_z, \\ \ddot{\theta} &= A_{21} * \tau_{xf} + A_{22} * \tau_{yf} + A_{23} * \tau_z, \\ \ddot{\psi} &= A_{31} * \tau_{xf} + A_{32} * \tau_{yf} + A_{33} * \tau_z,\end{aligned}\tag{5.21}$$

where τ_{xf} and τ_{yf} are the filtered torques. Figures 5.16 and 5.17 show τ_x (before filtration) and τ_{xf} (after filtration) divided by the desired inertia I_{xx_d} , respectively, compared to the measured acceleration Phi_{dd} . Figure 5.18 and 5.19 also show τ_y (before filtration) and τ_{yf} (after filtration) divided by the desired inertia I_{xx_d} , respectively, compared to the measured acceleration $Theta_{dd}$. It can be seen that after filtration, the two signals are overlapped. This indicates that if the filtered input torque along with the measured acceleration are used to estimate I_{xx} , the obtained estimate will be equal to I_{xx_d} accurately, as will be shown later. The same applies to the estimation of I_{yy} .

When an abrupt change in the quadrotor's mass occurs, a sudden change in the total thrust used to maintain the hovering state also appears. Thus, when the error between the real gravitational acceleration and the estimated one using

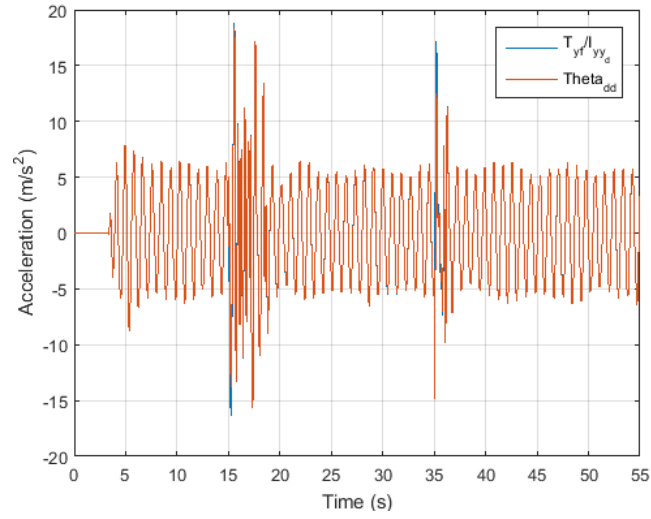


Figure 5.19: Filtered torque Vs. pitch measured acceleration in simulation

(5.17) exceeds a predefined threshold, the covariance matrix used in the RLS algorithm for the inertia estimation is reset to a value of $P = 10$ to increase the estimator's convergence rate. For instance, the error compared to a threshold of 0.4 is shown in Fig. 5.20, and the corresponding reset covariances for I_{xx} , I_{yy} , and I_{zz} estimation are shown in 5.21, 5.22, and 5.23, respectively.

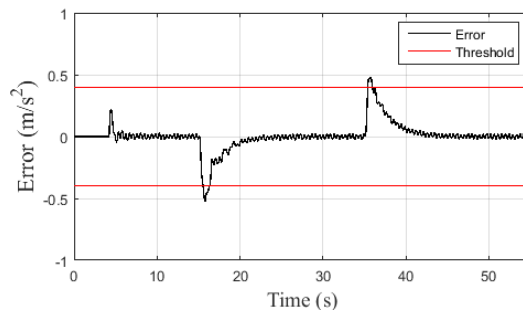


Figure 5.20: Detected error for covariance resetting in simulation

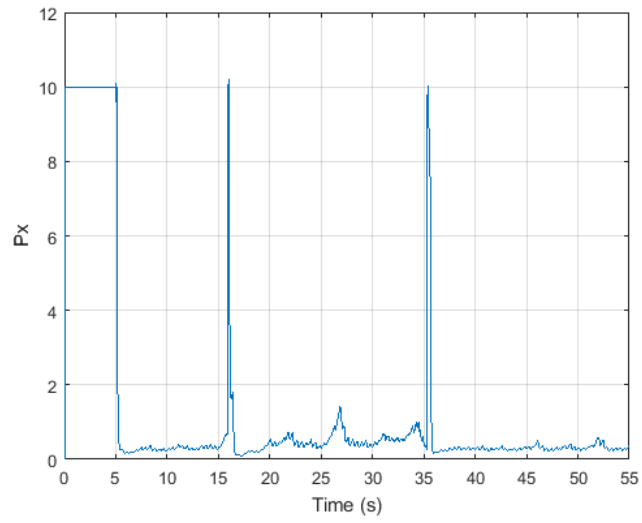


Figure 5.21: I_{xx} estimation auto-covariance in simulation

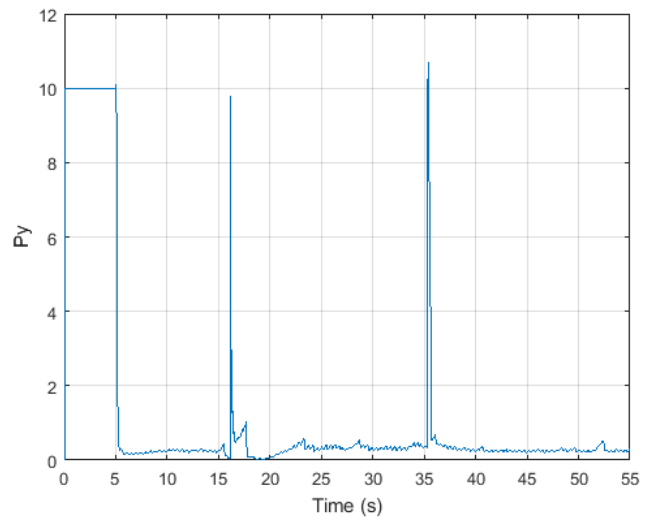


Figure 5.22: I_{yy} estimation auto-covariance in simulation

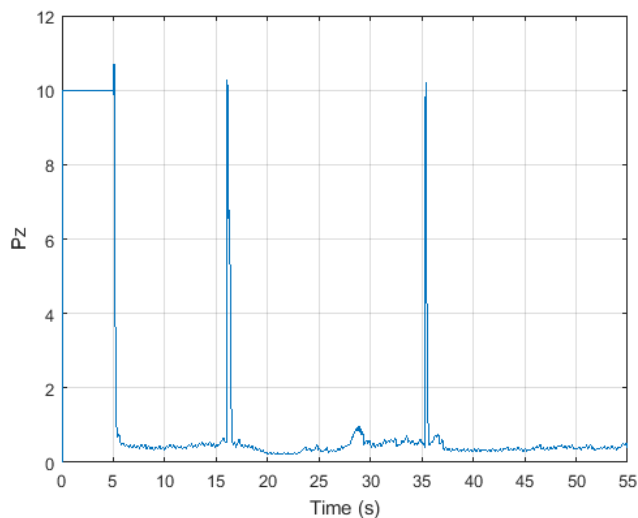
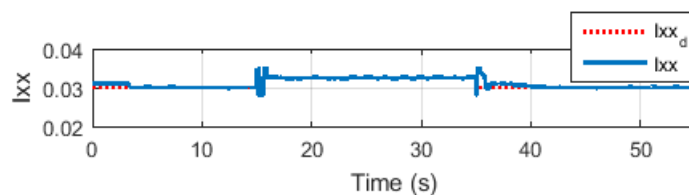
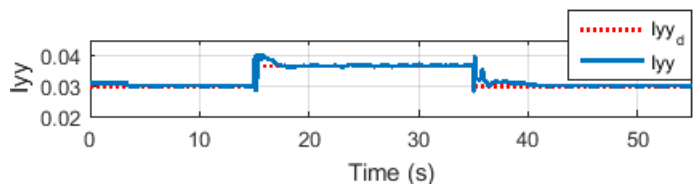


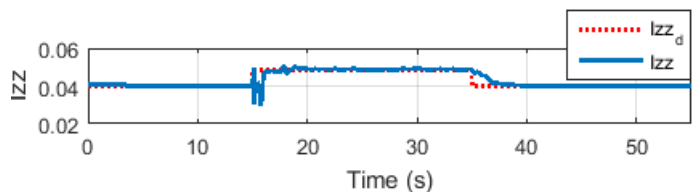
Figure 5.23: I_{zz} estimation auto-covariance in simulation



(a) Estimated parameter I_{xx}



(b) Estimated parameter I_{yy}



(c) Estimated parameter I_{zz}

Figure 5.24: Estimates of the inertia tensor diagonal elements in simulation

The parallel axis theorem is used to compute the quadrotor's new moment of inertia that is affected by the added mass, which is considered as a point mass. Hence, the new inertia tensor becomes:

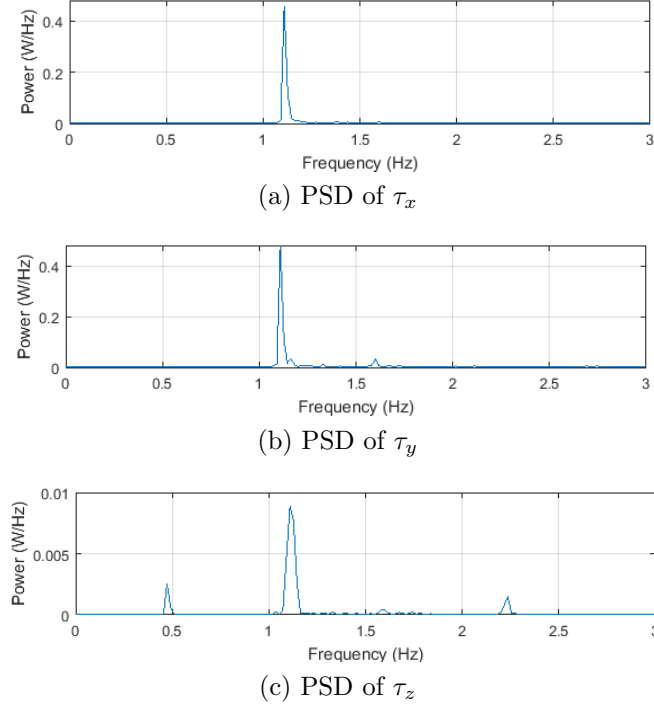


Figure 5.25: Power spectral densities (PSD) of the input torques in simulation

$$I_{total} = \begin{bmatrix} I_{xx_0} & 0 & 0 \\ 0 & I_{yy_0} & 0 \\ 0 & 0 & I_{zz_0} \end{bmatrix} + m_{add} \begin{bmatrix} r_y^2 + r_z^2 & -r_x r_y & -r_x r_z \\ -r_x r_y & r_x^2 + r_z^2 & -r_y r_z \\ -r_x r_z & -r_y r_z & r_x^2 + r_y^2 \end{bmatrix}, \quad (5.22)$$

where m_{add} is the added mass, and r_x , r_y , and r_z are its coordinates with respect to the quadrotor's geometric center. With an added mass of $0.1Kg$, the new inertia matrix is computed as follows:

$$I_{theoretical} = \begin{bmatrix} 0.0325 & -0.00375 & 0.00125 \\ -0.00375 & 0.0365 & 0.00075 \\ 0.00125 & 0.00075 & 0.0485 \end{bmatrix}.$$

The estimated inertia matrix as obtained via simulation is:

$$I_{estimated} = \begin{bmatrix} 0.03246 & -0.00371 & 0.00122 \\ -0.00371 & 0.03658 & 0.00094 \\ 0.00122 & 0.00094 & 0.049 \end{bmatrix}.$$

To evaluate the convergence rate and accuracy of the estimation method, the plots of the inertia tensor diagonal elements are shown in Fig. 5.24. As seen, when the mass is added, a fast transient response and small steady-state error are exhibited by the estimator. Since it does not take into account parametric

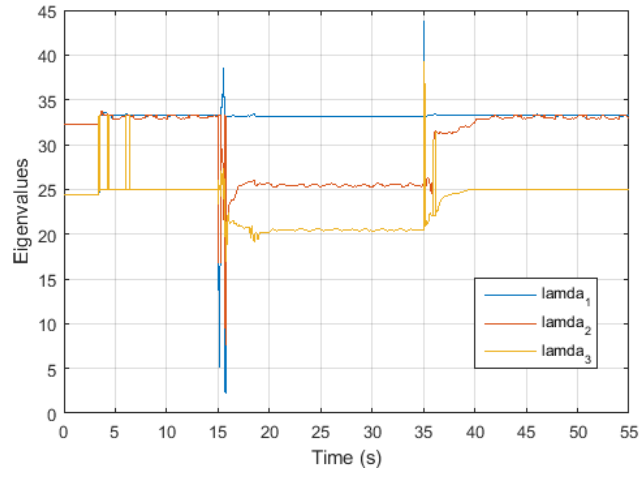


Figure 5.26: Eigenvalues of J

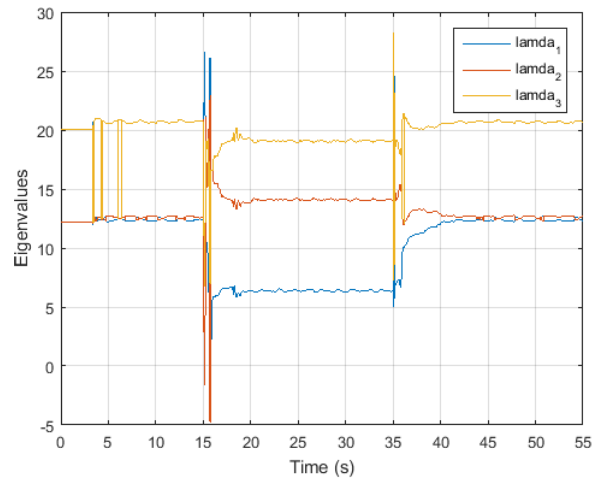


Figure 5.27: Eigenvalues of Y before correction

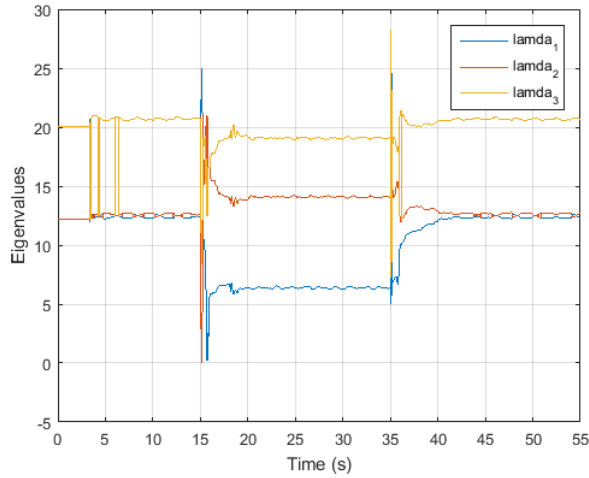


Figure 5.28: Eigenvalues of Y after correction

uncertainties and disturbances, small deviations and slightly diminished tracking performance when the mass is added appears in the identified parameters and are attributed to the fixed-gain PID controller. In fact, when the quadrotor does not adequately track the desired three Euler angles signals designed to provide sufficiently excited motions, the inputs' persistence of excitation will decrease, and the estimated parameters will swerve from their actual values. It is noted that, while designing such desired signals, the ability of the quadrotor to track them simultaneously should be taken into account. For instance, if the frequency or amplitude of the desired roll angle signal is chosen to be relatively much higher than those of the desired pitch and yaw angles, the quadrotor will provide poor tracking performance for the latter. As a result, the pitch and yaw motions will be less excited, and the parameters estimated using the roll regression equation will be more accurate than those estimated using the pitch and yaw regression equations. Similarly, if the frequencies and the amplitudes of the three desired signals were chosen to be all high, the quadrotor will not be able to track them simultaneously with adequate performance due to the coupling between these angles. Then, all the estimated inertia matrix values will be biased. Therefore, the amplitudes and frequencies of the desired Euler angles signals should be chosen in a compromised way such that they are not very low so that their corresponding motions are sufficiently excited while, on the other hand, they are not very high such that they provide the quadrotor the ability to track them simultaneously with adequate performance.

The accurate estimation results indicate that the input torques used in the identification process are indeed persistently exciting, which is established in Fig. 5.25 that shows the power spectral density (PSD) plots of τ_x , τ_y , and τ_z , respectively. The three input torques excite sufficient frequencies to accurately identify the three parameters in each linear regression equation given in (5.4).

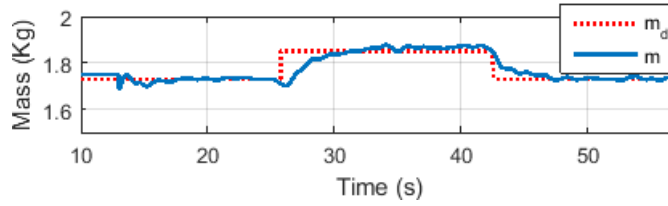


Figure 5.29: Quadrotor’s mass estimation in numerical simulation

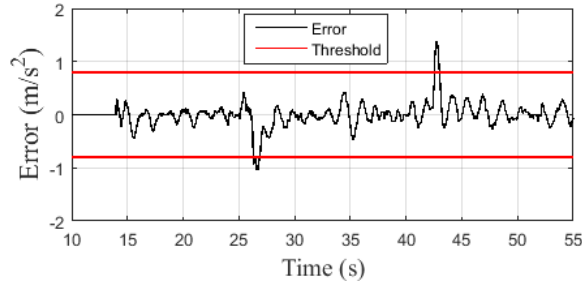


Figure 5.30: Detected error for covariance resetting in experiment

To assert the invertibility of the inertia tensor matrix inverse, conditions (4.6) and (4.15) are continuously verified by calculating their eigenvalues and checking that they are larger than zero at each time step. If not, the matrix obtained at the previous time step is used as the current inertia matrix inverse.

Figure 5.26 shows that the eigenvalues of J are positive over time guaranteeing condition (4.6). However, two eigenvalues of Y in condition (4.15), shown in Fig. 5.27, present negative values between time $t = 15$ and $t = 17$. After using the method explained in the previous paragraph, the eigenvalues are always larger than zero as shown in Fig. 5.28.

5.2.2 Experimental Validation

The QBall-2 quadrotor is used to validate the proposed estimation scheme experimentally. The testing sequence is started with the quadrotor hovering at an altitude of $1m$, then commanding oscillatory trajectories to each of its rotational degrees-of-freedom, independently. When the desired trajectories are simultaneously commanded, the quadrotor’s PID control system is unable to provide exact tracking performance due to coupling effects between the degrees of freedom. This tends to influence the estimation performance since the input torques do not perfectly correspond to the output accelerations, thus the obtained estimates may feature a slight bias. To circumvent this limitation, three independent experiments are performed where only one degree-of-freedom is excited at a time.

A mass of $0.1Kg$ is manually added (via hanging) at time $t \approx 25s$ at coordinates $r_x = 0.29m$, $r_y = 0.18m$, and $r_z = -0.06m$, and removed (via cutting

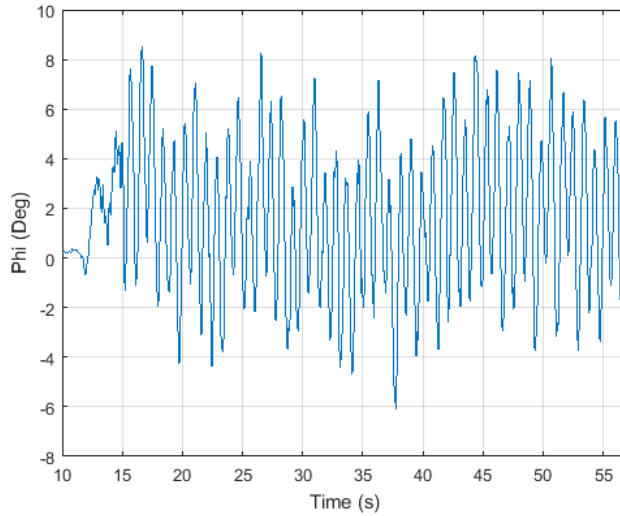


Figure 5.31: Output roll ϕ angle

its thread) at $t \approx 42s$. The quadrotor's mass is estimated by exciting the yaw dynamics while the quadrotor is in a hovering state. Figure 5.29 shows the mass estimation during the yaw excitation experiment, which demonstrates the accuracy of the estimator upon the addition and removal of the payload, and a comparable transient response relative to the simulation results.

To identify I_{xx} and I_{yy} , a sinusoidal wave of frequency $f = 7Hz$ and amplitude $A = 5^\circ$ is commanded as the desired roll and pitch trajectories, respectively. To identify I_{zz} , a sinusoidal wave with $f = 5Hz$ and $A = 7^\circ$ is commanded as a yaw trajectory, where the relatively lower frequency and higher amplitude are due to the yaw dynamics being slower than the roll and pitch dynamics of quadrotors. The corresponding obtained output angles in each experiment are shown in Fig. 5.31, 5.32, and 5.33, respectively. Since each degree of freedom is excited separately in each experiment, the off-diagonal elements cannot be estimated. Therefore, it would be more efficient to work in the future on finding a smart reference signal that excites all the degrees of freedom together while guaranteeing PE using pseudo-random binary signals (PRBS).

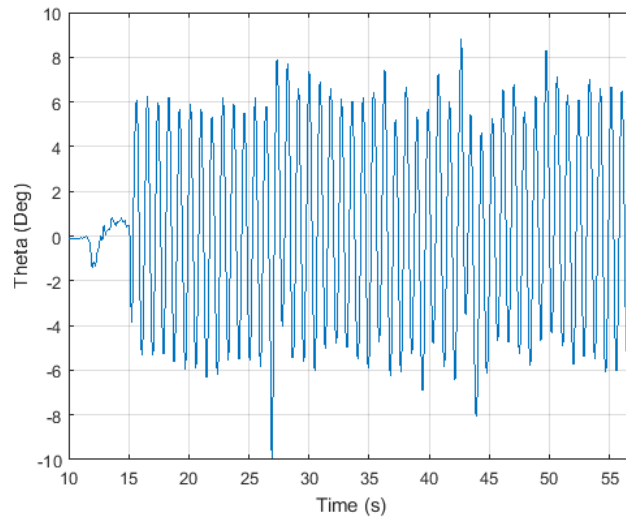


Figure 5.32: Output pitch θ angle

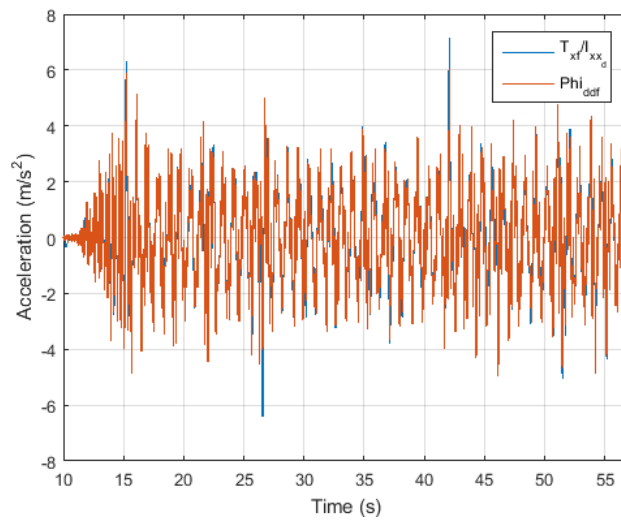


Figure 5.35: Filtered torque Vs. roll measured acceleration in experimentation

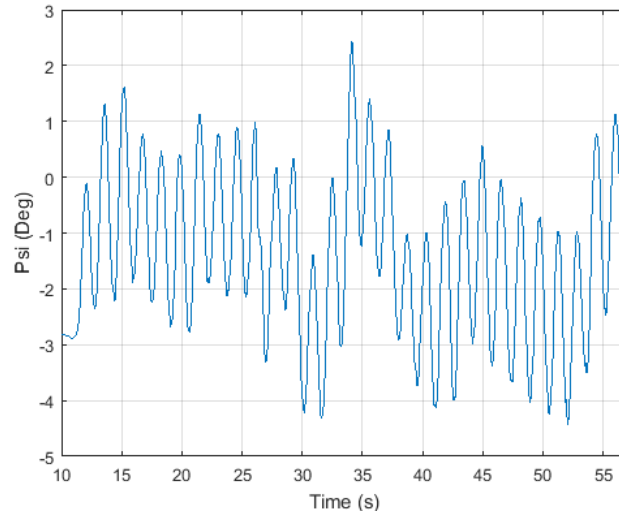


Figure 5.33: Output yaw ψ angle

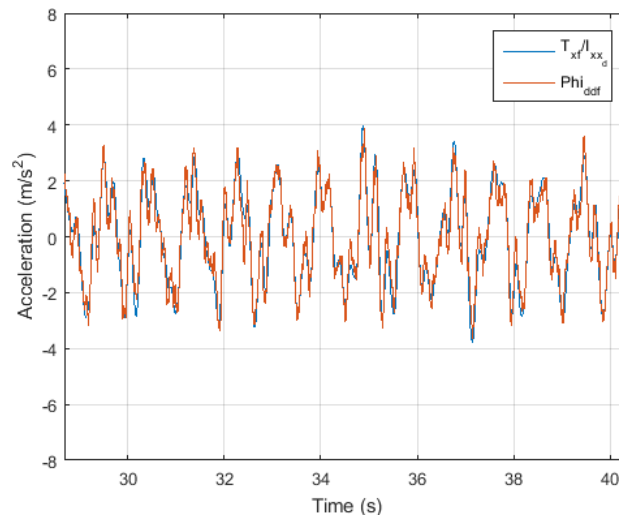


Figure 5.36: Filtered torque Vs. roll measured acceleration (Zoomed) in experimentation

As implemented in simulation, high-pass filters are also implemented in experimentation to remove the offset in the input torques caused by the mass addition. Furthermore, low-pass filters are added to remove the high frequency noise from the acceleration signals. As mentioned previously, filtration causes time delays between signals, thus by detecting these time delays the two signals are synchronized using a Delay block in Simulink. Figures 5.34 and 5.35 show τ_x divided by the desired inertia I_{xx_d} compared to the measured acceleration Phi_{dd} before filtration and after filtration, respectively. A zoomed part from Fig. 5.35 is presented in Fig 5.36, which demonstrates how filtration helps to get overlapped

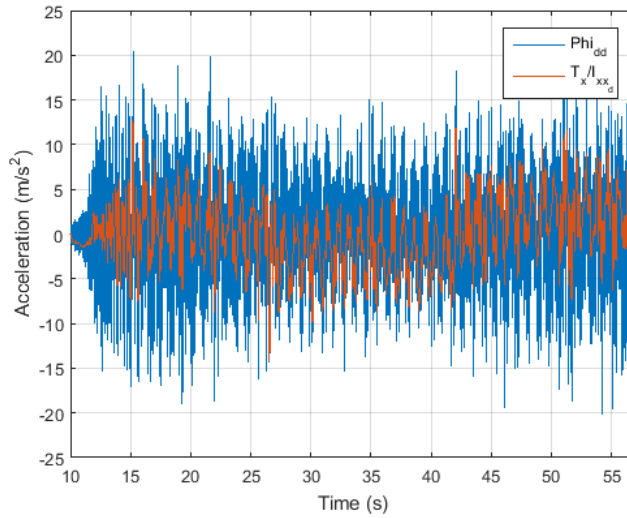


Figure 5.34: Non filtered torque Vs. roll measured acceleration in experimentation

estimated and measured accelerations. This means that accurate estimation of I_{xx} will be obtained during the experiment. Figures 5.37 and 5.38 also show τ_y divided by the desired inertia I_{yy_d} compared to the measured acceleration Θ_{dd} before filtration and after filtration, respectively. The overlapped measured and estimated accelerations shown in the zoomed Fig. 5.39 of Fig. 5.35 indicates that an accurate estimation of I_{yy} will also be obtained.

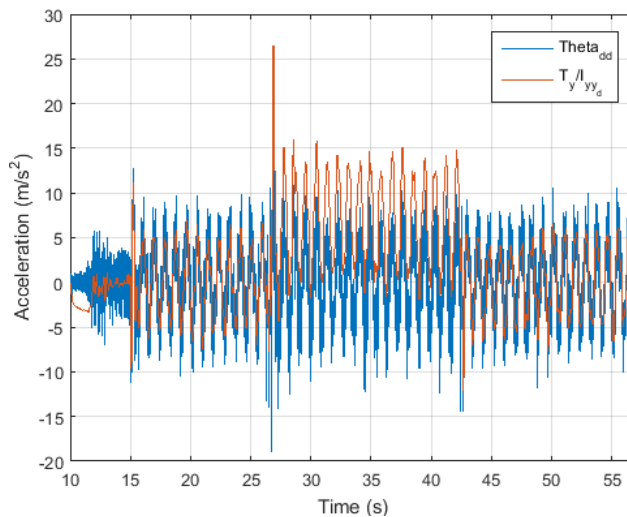


Figure 5.37: Non filtered torque Vs. pitch measured acceleration in experimentation

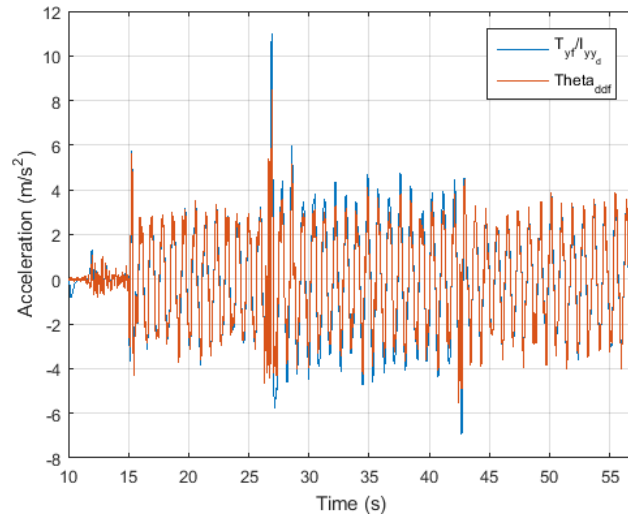


Figure 5.38: Filtered torque Vs. pitch measured acceleration

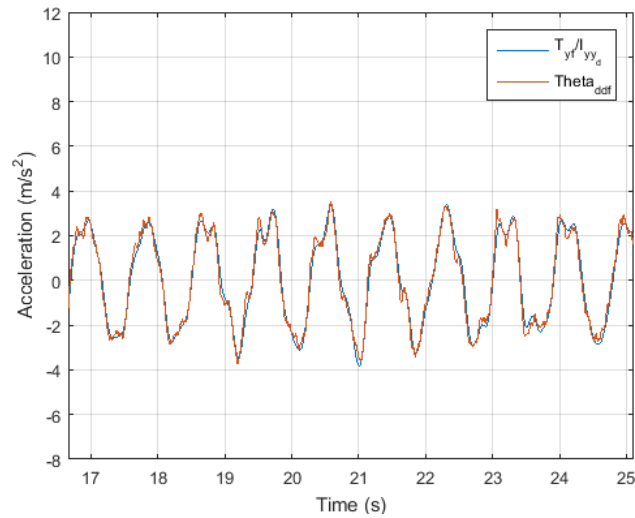


Figure 5.39: Filtered torque Vs. pitch measured acceleration (Zoomed) in experimentation

Since no offset in τ_z is induced by the mass addition, only low-pass filters to remove the high frequency noise are needed. After filtration and synchronization, the filtered estimated and measured yaw accelerations are shown in Fig. 5.40. The zoomed signals shown in Fig. 5.41 elaborate how the overlapped signals will result in an accurate estimate of I_{zz} in the yaw experiment.

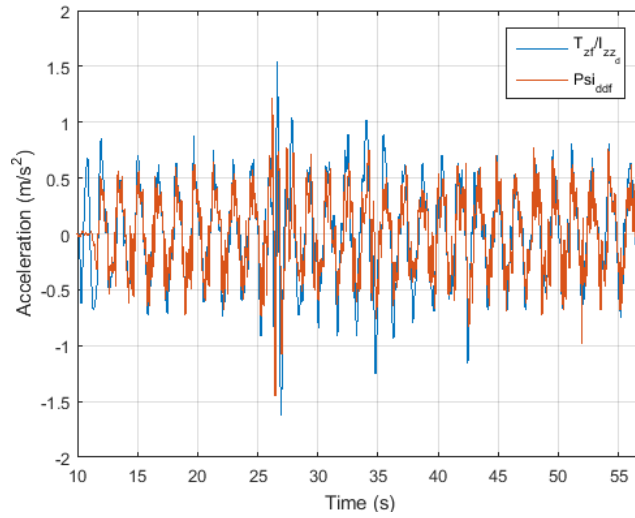


Figure 5.40: Filtered torque Vs. yaw measured acceleration in experimentation

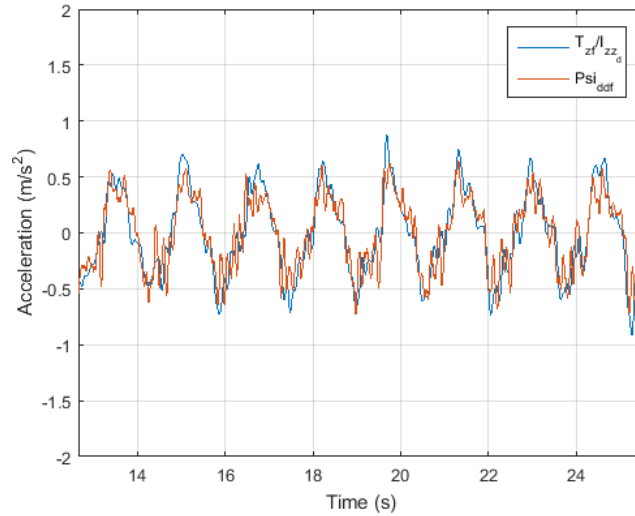


Figure 5.41: Filtered torque Vs. yaw measured acceleration (Zoomed) in experimentation

Covariance resetting is applied per the method in section 4.3 with an error threshold of 0.8, as shown in Fig. 5.30, and the corresponding reset covariances for I_{xx} , I_{yy} , and I_{zz} estimation are shown in Fig. 5.42, Fig. 5.43, and Fig. 5.44, respectively.

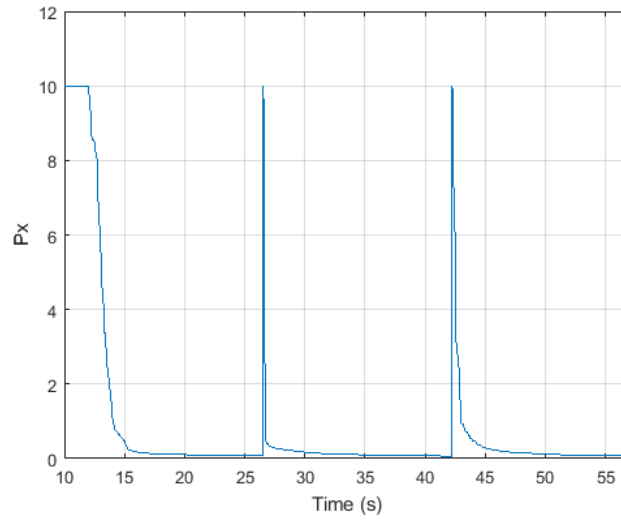


Figure 5.42: I_{xx} estimation auto-covariance in experimentation

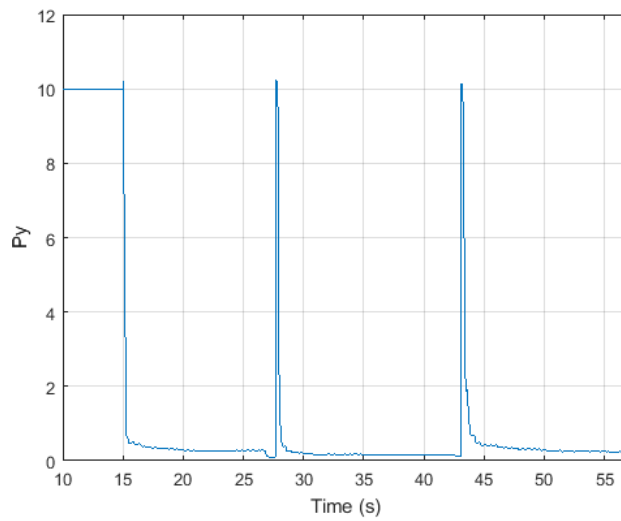


Figure 5.43: I_{yy} estimation auto-covariance in experimentation

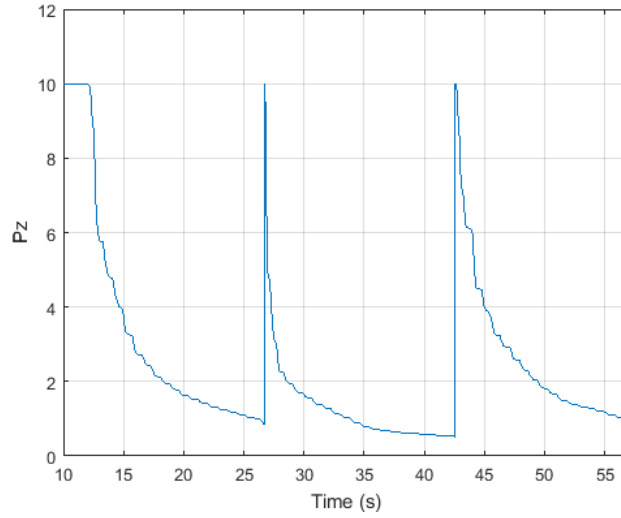
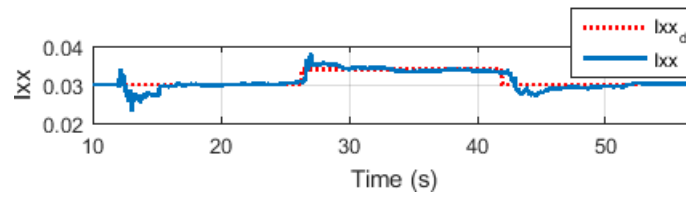
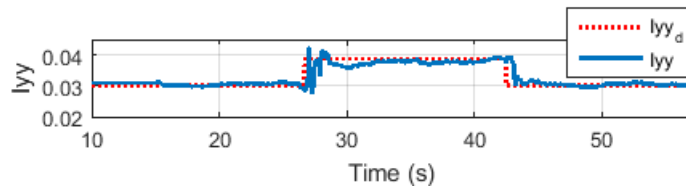


Figure 5.44: I_{zz} estimation auto-covariance in experimentation

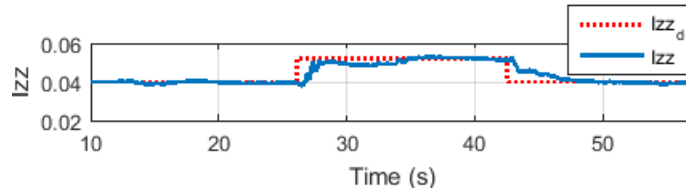
The estimates of the diagonal terms of the inertia tensor obtained during the three experiments are shown in Fig. 5.45.



(a) Estimated parameter I_{xx}



(b) Estimated parameter I_{yy}



(c) Estimated parameter I_{zz}

Figure 5.45: Estimates of the inertia tensor diagonal elements in experiment

It is noticed that the experimentally obtained estimates show strong correlation with the simulation results relative to high accuracy and fast convergence.

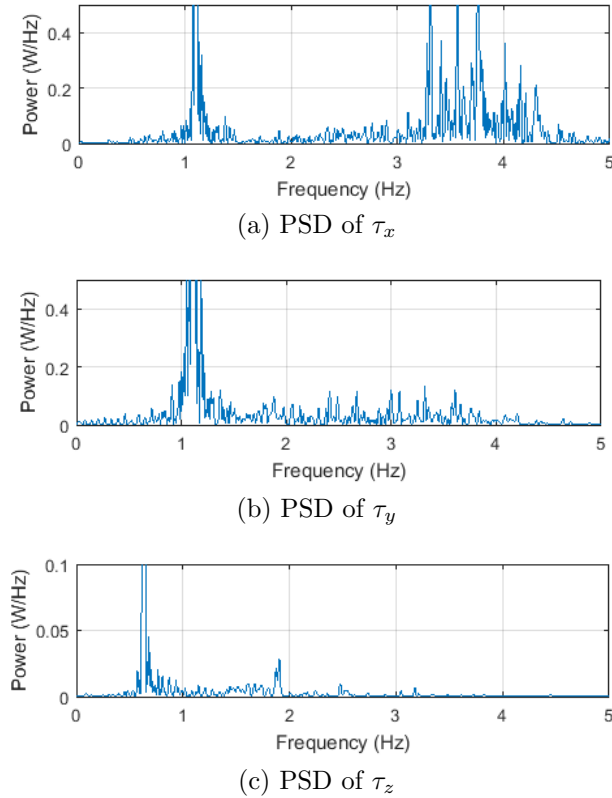


Figure 5.46: Power spectral densities (PSD) of the input torques in experiment

Although the input torques are persistently exciting, as illustrated by their PSDs in Fig. 5.46, a small bias is observed in the estimates, which is caused by several modelling inaccuracies, nonlinearities, and uncertainties such as the battery drain effect, drag and thrust coefficients, and state coupling, to name a few. In fact, modelling inaccuracies include, for instance, the blade flapping, ground effect, and ceiling effect that are not incorporated into the model. Furthermore, the nonlinear terms in (3.9) are neglected, while they are present in the real system. In addition, the battery drain model is considered linear whereas it is nonlinear on the QBall-2. It is noted that the torque τ_z is not affected by the battery voltage only, but also its discharging capacity that varies with time given that the torque generated by a DC motor is directly proportional to the current drawn by the motor. Thus, as an improvement, a current sensor can be added to the system to identify the battery discharging behaviour. Last but not least, in the model used for the identification, the Euler degrees-of-freedom are considered decoupled in the linear dynamic model while a strong coupling between them exists in the system as exhibited in its nonlinear model. However, despite such inaccurately modeled effects, the moment of inertia estimates are within 5% of their true values.

Chapter 6

Conclusion

In this work, the mass and all elements of the inertia tensor matrix of a package delivery quadrotor are estimated using recursive least squares algorithm. Covariance resetting is added to the algorithm to speed up the convergence rate and to accommodate to the abrupt changes applied on the system. To estimate the mass, the quadrotor is operated in its hover state; The input is the total thrust generated by the motors and the output is the gravitational acceleration. Whereas, to estimate the inertia tensor matrix, the input signals are the applied torques on the quadrotor's three rotational degrees-of-freedom and the output data are the corresponding rotational accelerations. The input torques are calculated from the voltages applied on the motors using DC motor's first order model and the thrust and drag coefficients. The Lithium battery drain effect is also implemented in the estimation scheme to take into consideration the gradual voltage drop presented by the batteries. The estimator is validated via numerical simulation and experimental testing on a physical quadrotor system and on a hover quadrotor platform. The hover's DC motors first order transfer is identified using an obstacle sensor and the thrust and torque coefficients are estimated using a force sensor. On the other, those of the QBall-2 quadrotor are provided by its datasheet. As a quadrotor's dynamic parameters present physical meaning, several conditions are attained during estimation to get physically consistent estimates. Such conditions are the positive definiteness of the inertia tensor and the triangle inequality that should be met by its eigenvalues. The obtained results demonstrate the accuracy, efficiency, consistency, and convergence rate of the proposed identification scheme. Future work entails integrating the identification scheme into controller mapping scheme or into an indirect adaptive control system to achieve output tracking performance when the quadrotor picks up, carries, and drops off delivery packages of variable masses and shapes. A current sensor may be added to the system to adequately identify the battery current drain that affects the motors generated torques. Furthermore, a method to simultaneously estimate the three rows of the inertia tensor matrix in one experiment may be studied. This would save more time than when each degree of

freedom is excited independently. The obtained estimated parameters may also be used in health monitoring algorithms, and employed in quality control systems for detecting payload characteristics.

Bibliography

- [1] “Quanser Inc.” <http://www.quanser.com>, 2019.
- [2] S. Norouzi Ghazbi, Y. Aghli, M. Alimohammadi, and A. A. Akbari, “Quadrotors unmanned aerial vehicles: A review.,” *International Journal on Smart Sensing & Intelligent Systems*, vol. 9, no. 1, 2016.
- [3] T. Tomic, K. Schmid, P. Lutz, A. Domel, M. Kassecker, E. Mair, I. L. Grixia, F. Ruess, M. Suppa, and D. Burschka, “Toward a fully autonomous uav: Research platform for indoor and outdoor urban search and rescue,” *IEEE robotics & automation magazine*, vol. 19, no. 3, pp. 46–56, 2012.
- [4] A. Barrientos, J. Colorado, J. d. Cerro, A. Martinez, C. Rossi, D. Sanz, and J. Valente, “Aerial remote sensing in agriculture: A practical approach to area coverage and path planning for fleets of mini aerial robots,” *Journal of Field Robotics*, vol. 28, no. 5, pp. 667–689, 2011.
- [5] A. Benallegue, A. Mokhtari, and L. Fridman, “High-order sliding-mode observer for a quadrotor uav,” *International Journal of Robust and Nonlinear Control: IFAC-Affiliated Journal*, vol. 18, no. 4-5, pp. 427–440, 2008.
- [6] H. Huang, G. M. Hoffmann, S. L. Waslander, and C. J. Tomlin, “Aerodynamics and control of autonomous quadrotor helicopters in aggressive maneuvering,” in *2009 IEEE international conference on robotics and automation*, pp. 3277–3282, IEEE, 2009.
- [7] S. B. Monfared, A. Kalhor, and M. A. Atashgah, “Robust h control for path tracking of a quadrotor through estimation of system parameters,” in *2016 4th International Conference on Robotics and Mechatronics (ICROM)*, pp. 337–342, IEEE, 2016.
- [8] L. Lennart, “System identification: theory for the user,” *PTR Prentice Hall, Upper Saddle River, NJ*, pp. 1–14, 1999.
- [9] L. Derafa, T. Madani, and A. Benallegue, “Dynamic modelling and experimental identification of four rotors helicopter parameters,” in *2006 IEEE International Conference on Industrial Technology*, pp. 1834–1839, IEEE, 2006.

- [10] A. Chovancová, T. Fico, L. Chovanec, and P. Hubinsk, “Mathematical modelling and parameter identification of quadrotor (a survey),” *Procedia Engineering*, vol. 96, pp. 172–181, 2014.
- [11] M. De Oliveira, “Modeling, identification and control of a quadrotor aircraft,” *Czech Technical University, Prague*, 2011.
- [12] M. Shaqura and J. S. Shamma, “An automated quadcopter cad based design and modeling platform using solidworks api and smart dynamic assembly,” in *ICINCO (2)*, pp. 122–131, 2017.
- [13] I. Stanculeanu and T. Borangiu, “Quadrotor black-box system identification,” *World Academy of Science, Engineering and Technology*, vol. 5, pp. 276–279, 2011.
- [14] R. Schreurs, S. Weiland, H. Tao, Q. Zhang, J. Zhu, Y. Zhu, and C. Xu, “Open loop system identification for a quadrotor helicopter system,” in *2013 10th IEEE International Conference on Control and Automation (ICCA)*, pp. 1702–1707, IEEE, 2013.
- [15] <http://www.it.uu.se/edu/course/homepage/systemid/vt12/ch8.pdf>.
- [16] W. Wei, N. Schwartz, and K. Cohen, “Frequency-domain system identification and simulation of a quadrotor controller,” in *AIAA Modeling and Simulation Technologies Conference*, p. 1342, 2014.
- [17] H.-r. Qi and X.-h. Qi, “Key parameter identification of quad-rotor aircraft system based on cifer algorithm,” in *2017 2nd International Conference on Materials Science, Machinery and Energy Engineering (MSMEE 2017)*, Atlantis Press, 2017.
- [18] L. Yang and J. Liu, “Parameter identification for a quadrotor helicopter using pso,” in *52nd IEEE Conference on Decision and Control*, pp. 5828–5833, IEEE, 2013.
- [19] M. T. Alkowitz, V. Becerra, and W. Holderbaum, “Body-centric modelling, identification, and acceleration tracking control of a quadrotor uav,” *International journal of modelling, identification and control*, vol. 24, no. 1, pp. 29–41, 2015.
- [20] J. Muliadi, R. Langit, and B. Kusumoputro, “Estimating the uav moments of inertia directly from its flight data,” in *2017 15th International Conference on Quality in Research (QiR): International Symposium on Electrical and Computer Engineering*, pp. 190–196, IEEE, 2017.

- [21] D. Ho, J. Linder, G. Hendeby, and M. Enqvist, “Mass estimation of a quadcopter using imu data,” in *2017 International Conference on Unmanned Aircraft Systems (ICUAS)*, pp. 1260–1266, IEEE, 2017.
- [22] X. Lei and Y. Du, “A linear domain system identification for small unmanned aerial rotorcraft based on adaptive genetic algorithm,” *Journal of Bionic Engineering*, vol. 7, no. 2, pp. 142–149, 2010.
- [23] D. Sonntag, “A study of quadrotor modelling,” 2011.
- [24] Y. Ameho, F. Niel, F. Defaÿ, J.-M. Biannic, and C. Bérard, “Adaptive control for quadrotors,” in *2013 IEEE International Conference on Robotics and Automation*, pp. 5396–5401, IEEE, 2013.
- [25] R. Mahony, V. Kumar, and P. Corke, “Multirotor aerial vehicles: Modeling, estimation, and control of quadrotor,” *IEEE robotics & automation magazine*, vol. 19, no. 3, pp. 20–32, 2012.
- [26] D. Schafroth, C. Bermes, S. Bouabdallah, and R. Siegwart, “Modeling, system identification and robust control of a coaxial micro helicopter,” *Control Engineering Practice*, vol. 18, no. 7, pp. 700–711, 2010.
- [27] K. Amelin, S. Tomashevich, and B. Andrievsky, “Recursive identification of motion model parameters for ultralight uav,” *IFAC-PapersOnLine*, vol. 48, no. 11, pp. 233–237, 2015.
- [28] V. Wüest, V. Kumar, and G. Loianno, “Online estimation of geometric and inertia parameters for multirotor aerial vehicles,” in *2019 International Conference on Robotics and Automation (ICRA)*, pp. 1884–1890, IEEE, 2019.
- [29] R. López, S. Salazar, I. Gonzalez-Hernandez, and R. Lozano, “Real-time parameters identification for a quad-rotor mini-aircraft using adaptive control,” in *2014 International Conference on Unmanned Aircraft Systems (ICUAS)*, pp. 499–505, IEEE, 2014.
- [30] J. Zhao, X. Wang, G. Gao, J. Na, H. Liu, and F. Luan, “Online adaptive parameter estimation for quadrotors,” *Algorithms*, vol. 11, no. 11, p. 167, 2018.
- [31] C. D. Sousa and R. Cortesao, “Physical feasibility of robot base inertial parameter identification: A linear matrix inequality approach,” *The International Journal of Robotics Research*, vol. 33, no. 6, pp. 931–944, 2014.
- [32] N. Michael, D. Mellinger, Q. Lindsey, and V. Kumar, “The grasp multiple micro-uav testbed,” *IEEE Robotics & Automation Magazine*, vol. 17, no. 3, pp. 56–65, 2010.

- [33] “Foreword to the third edition,” in *DC Motors, Speed Controls, Servo Systems (Third Edition)* (E.-C. CORPORATION, ed.), p. xv, Pergamon, third edition ed., 1972.
- [34] F. H. Guidi *et al.*, *Open and closed loop model identification and validation*. PhD thesis, University of Pretoria, 2009.
- [35] U. Forssell and L. Ljung, “Closed-loop identification revisited,” *Automatica*, vol. 35, no. 7, pp. 1215–1241, 1999.
- [36] U. Forssell, *Closed-loop identification: Methods, theory, and applications*. PhD thesis, Linköping University Electronic Press, 1999.
- [37] L. Ljung, “Prediction error estimation methods,” *Circuits, Systems and Signal Processing*, vol. 21, no. 1, pp. 11–21, 2002.
- [38] B. Huang and S. L. Shah, “Closed-loop identification: a two step approach,” *Journal of Process Control*, vol. 7, no. 6, pp. 425–438, 1997.
- [39] G. C. Goodwin and R. L. Payne, *Dynamic system identification: experiment design and data analysis*. Academic press, 1977.
- [40] L. Ljung and T. Söderström, *Theory and practice of recursive identification*. MIT press, 1983.
- [41] K. J. Hunt, “A survey of recursive identification algorithms,” *Transactions of the Institute of Measurement and Control*, vol. 8, no. 5, pp. 273–278, 1986.
- [42] Ö. F. Durdu, “A comparison of recursive least squares estimation and kalman filtering for flow in open channels,” *Turkish Journal of Engineering and Environmental Sciences*, vol. 29, no. 3, pp. 171–183, 2005.
- [43] V. Ranganathan, G. Prabha, and K. Narayanankutty, “Constant modulus hybrid recursive and least mean squared algorithm performance comparable to unscented kalman filter for blind beamforming,” in *2016 IEEE Annual India Conference (INDICON)*, pp. 1–4, IEEE, 2016.
- [44] K. J. Åström and B. Wittenmark, *Adaptive control*. Courier Corporation, 2013.
- [45] K. Yoshida and W. Khalil, “Verification of the positive definiteness of the inertial matrix of manipulators using base inertial parameters,” *The International Journal of Robotics Research*, vol. 19, no. 5, pp. 498–510, 2000.
- [46] S. Traversaro, S. Brossette, A. Escande, and F. Nori, “Identification of fully physical consistent inertial parameters using optimization on manifolds,” in *2016 IEEE/RSJ International Conference on Intelligent Robots and Systems (IROS)*, pp. 5446–5451, IEEE, 2016.

- [47] C. D. Sousa and R. Cortesao, “Inertia tensor properties in robot dynamics identification: A linear matrix inequality approach,” *IEEE/ASME Transactions on Mechatronics*, vol. 24, no. 1, pp. 406–411, 2019.
- [48] S. Bouabdallah, A. Noth, and R. Siegwart, “Pid vs lq control techniques applied to an indoor micro quadrotor,” in *2004 IEEE/RSJ International Conference on Intelligent Robots and Systems (IROS)(IEEE Cat. No. 04CH37566)*, vol. 3, pp. 2451–2456, IEEE, 2004.
- [49] A. Abdulghany, “Generalization of parallel axis theorem for rotational inertia,” *American Journal of Physics*, vol. 85, no. 10, pp. 791–795, 2017.
- [50] “Gumstix.” <http://gumstix.com>.
- [51] “Stmicroelectronics l3g4200d 3-axis gyroscope.” http://www.st.com/web/catalog/sense_power/FM89/SC1288/PF250373, 2019.